Geoderma 436 (2023) 116531

Contents lists available at ScienceDirect

Geoderma

journal homepage: www.elsevier.com/locate/geoderma

Pedogenic pathways and deep weathering controls on soil organic carbon in Pacific Northwest forest soils

Brooke D. Hunter [a,*], Joshua J. Roering [a], Peter C. Almond [b], Oliver A. Chadwick [c], Matthew L. Polizzotto [a], Lucas C.R. Silva [d]

[a] Department of Earth Sciences, University of Oregon, Eugene, OR, USA
[b] Department of Soil and Physical Sciences, Lincoln University, Canterbury, New Zealand
[c] Department of Geography, University of California, Santa Barbara, CA, USA
[d] Environmental Studies Program, Department of Biology, Institute of Ecology & Evolution, University of Oregon, Eugene, OR 97405, USA

ARTICLE INFO

Handling Editor: Karen Vancampenhout

Keywords:
Soil organic carbon
Weathering
Pedogenesis
Poorly crystalline minerals

ABSTRACT

Characterizing the distribution and dynamics of organic carbon in soil is critical for quantifying changes in the global carbon cycle. In particular, weathering controls on near-surface and deep (>1 m) soil organic carbon (SOC) dynamics have been proposed but limited data prevents us from predicting SOC over topographically complex landscapes and quantifying how changes in climate and perturbations, such as wildfire or land management, influence SOC stocks. To advance our understanding of how weathering alters soil geochemistry and influences SOC storage, we synthesize previous data with a new analysis of the Siuslaw River soil chronosequence from terraces in the Oregon Coast Range, a region that harbors the richest SOC inventories in the continental US. We analyze how the relationships between soil geochemistry, physical properties, and SOC storage vary with weathering status and pathways across soils that span 0.041 to 990 kyr and vary in depth from 1 m to >10 m. To distinguish the key properties and processes influencing SOC storage at different depths, we break our analysis into three depth intervals: 0–30, 30–100, and >100 cm. Our results suggest that the processes that control SOC stocks vary systematically with time and depth owing to weathering impacts on soil properties and pedogenic development. At 30 kyr we observe a peak in SOC stock in the top 100 cm coincident with a peak in oxalate extractable Al and Fe concentrations, representing secondary poorly crystalline minerals, which is consistent with previous studies. We also observe a decline in shallow SOC stock for >30 kyr soils as poorly crystalline minerals are replaced by more stable crystalline forms and soils become clay dominated. At 120 kyr, SOC below 100 cm starts to contribute significantly to the total SOC profile inventory and by 990 kyr, this fraction composes >40% of the total SOC stock. Taken together, our results indicate that total SOC stock increases with soil age as the increased intensity of bedrock weathering deepens the critical zone, creating accommodation space for deep SOC storage. These findings reveal the intimate link between poorly crystalline minerals and SOC and suggest that systematic analysis of soil development in the critical zone provides a first-order constraint on SOC stocks.

1. Introduction

The pedosphere stores ~2,400 Pg of organic carbon (OC) in the upper 2 m (Batjes, 2014), which is more than the biosphere and atmosphere combined, making it the largest terrestrial pool of OC (Jobbágy and Jackson, 2000; Kirschbaum, 2000; Le Quéré et al., 2015; Tarnocai et al., 2009). The relative amount of OC in the pedosphere compared to the atmosphere and biosphere, means small changes in soil organic carbon (SOC) can influence atmospheric CO_2 and global carbon dynamics (Conant et al., 2011; Minasny et al., 2017). However, uncertainty in the distribution, stability, and dynamics of organic carbon in the soil limits our understanding of the global carbon cycle and how

Abbreviations: SOC, soil organic carbon; MAOC, mineral-associated organic carbon; POC, particulate organic carbon; SRC, Siuslaw River Chronosequence; PCM, poorly crystalline mineral.

* Corresponding author.
E-mail addresses: bhunter2@uoregon.edu (B.D. Hunter), jroering@uoregon.edu (J.J. Roering), Peter.Almond@lincoln.ac.nz (P.C. Almond), ochadwick@ucsb.edu (O.A. Chadwick), mpolizzo@uoregon.edu (M.L. Polizzotto).

https://doi.org/10.1016/j.geoderma.2023.116531
Received 10 October 2022; Received in revised form 11 April 2023; Accepted 19 May 2023
Available online 7 June 2023

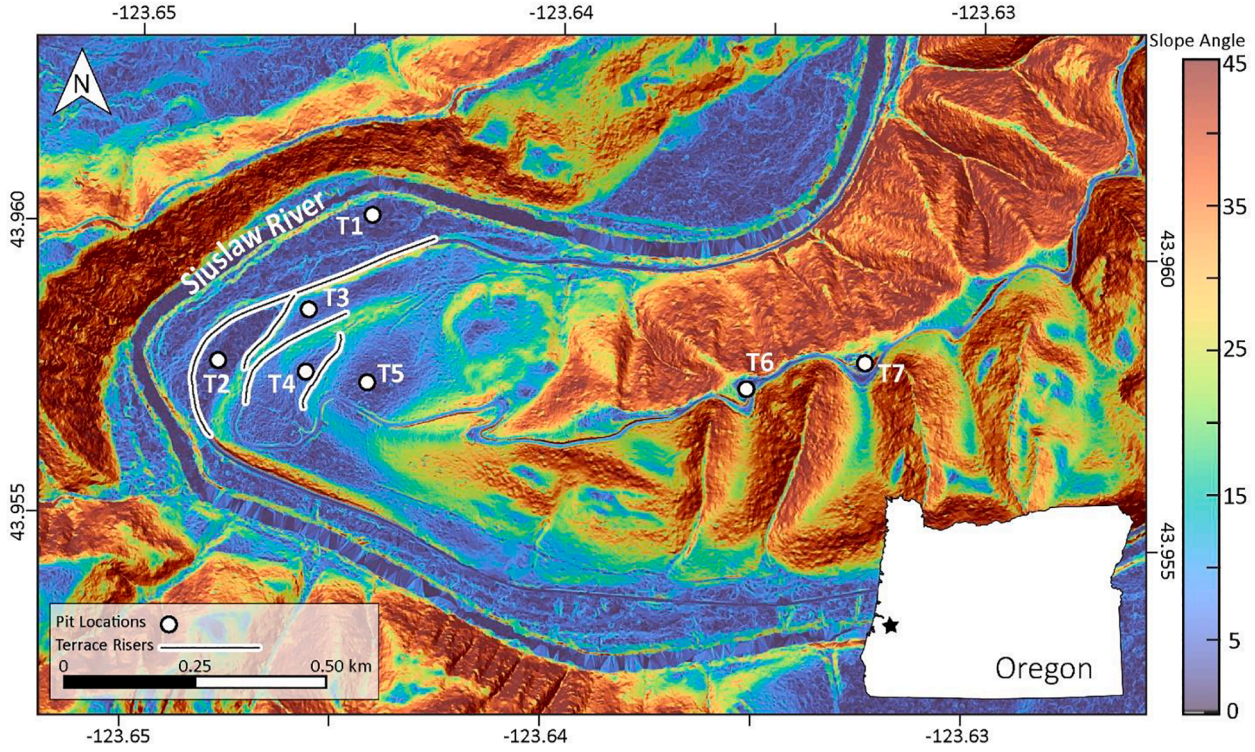

Fig. 1. Map of terrace locations for soil chronosequence over slope angle map modified from Almond et at. (2007). Terrace risers (white lines) and soil pit locations (black dots) represent sites of soils detailed in Almond et al. (2007).

Table 1
Site characteristics.

Terrace	Age (kyr)	Elevation (m)[e]	Depth of weathering (cm)[f]	MAP (mm)[g]	MAAT (°C)[g]
T1a	0.041[a]	85.5*	40	1,800	10.5
T1b	1[b]	85.5*	77	1,800	10.5
T2	30[c]	89.0	109	1,900	11
T3	69[d]	94.3	260	1,900	11
T4	140[d]	106.9	310	2,400	11
T5	200[d]	117.6	460	2,400	11
T6	908[d]	248.9	>910	2,550	9.5
T7	990[d]	263.8	>1,100	2,550	9.5

[a] T1a age is based on the occurrence of a significant flood in 1964. Samples were collected in 2005 so we applied an age of 41 years;
[b] T1 age of 3.5kyr was based on radiocarbon dating of detrital charcoal from Almond et al., (2007). We estimated an age for T1b by assuming it is younger than the fourth buried soil;
[c] from Almond et al. (2007), based on radiocarbon dating of detrital charcoal;
[d] from Almond et al. (2007), based on elevation, uplift rates and back calculation from incision rates;
[e] from Almond et al. (2007), field work with GPS;
[f] from Almond et al. (2007), equivalent to base of saprolite;
[g] from Soil Survey of Land County Area, Patching, W.R., (1987).

perturbations, such as wildfire or land management, may influence SOC stocks.

While many SOC studies focus on climatic, biologic, or lithologic controls on SOC storage (Silva and Lambers, 2021); weathering on millennial and longer timescales plays a key role in the development of soil ecosystem properties that modulate SOC storage (Doetterl et al., 2018; Hemingway et al., 2019; Schmidt et al., 2011). In addition to the chemical and molecular composition of soil organic matter (SOM) influencing SOC longevity itself (Kögel-Knabner et al., 2008; Lavallee et al., 2020; Six et al., 2000), soil texture, soil chemistry, thickness, aggregate abundance, and mineralogy set the accommodation space and protection mechanisms necessary for SOC storage (Kramer and Chadwick, 2016; Lehmann et al., 2020; Masiello et al., 2004; Slessarev et al., 2022). In general, these soil properties depend on the rates of fresh mineral supply (soil production), weathering, and erosion (Doetterl et al., 2016; Mudd and Yoo, 2010). Over millennia, these processes control soil properties required for significant SOC storage suggesting that analysis and quantification of soil development can advance our understanding of the persistence and preservation of SOC (Lehmann et al., 2020).

Chronosequence studies are often used to investigate the trajectory of pedogenesis on millennial timescales through analysis of soil mineralogy and physical properties (Almond et al., 2007; Birkeland, 1992; Harden, 1982; Lawrence et al., 2015; Lilienfein et al., 2003; Lindeburg et al., 2013; Mainka et al., 2022; Masiello et al., 2004; Torn et al., 1997; Vreeken, 1975, 1975; Walker et al., 2010). To isolate the effect of time, chronosequence studies examine soils across landforms with consistent vegetation (net primary production input), climate and parent material (Almond et al., 2007; Baisden et al., 2002; Kramer and Chadwick, 2016; Masiello et al., 2004). These landforms often originate from marine, fluvial, or glacial deposits or lava flows and are assumed to experience negligible surface erosion, and therefore highlight biogeochemical changes over time. From these studies we understand that as soils age, continual physical and chemical weathering breaks down and converts primary minerals to secondary ones. For soils in humid environments, this causes an increase in silt- and clay- sized minerals and greater abundance of reactive pedogenic products such as Fe-oxides and Al-oxyhydroxides (Chadwick and Chorover, 2001; Lawrence et al., 2015), and higher aggregate abundance and stability (Wei et al., 2016) in the soil matrix. The patterns and timescales of soil property development and SOC storage play an integral role in connecting the trajectory of soil development and SOC stocks (Baldock and Skjemstad, 2000; Lawrence et al., 2021).

Clay-sized particles have long been hypothesized to be one of the most important soil properties conducive to mineral associated organic carbon (MAOC) protection (Kleber et al., 2021; Six et al., 2000), by providing large amounts of surface area to form organo-mineral

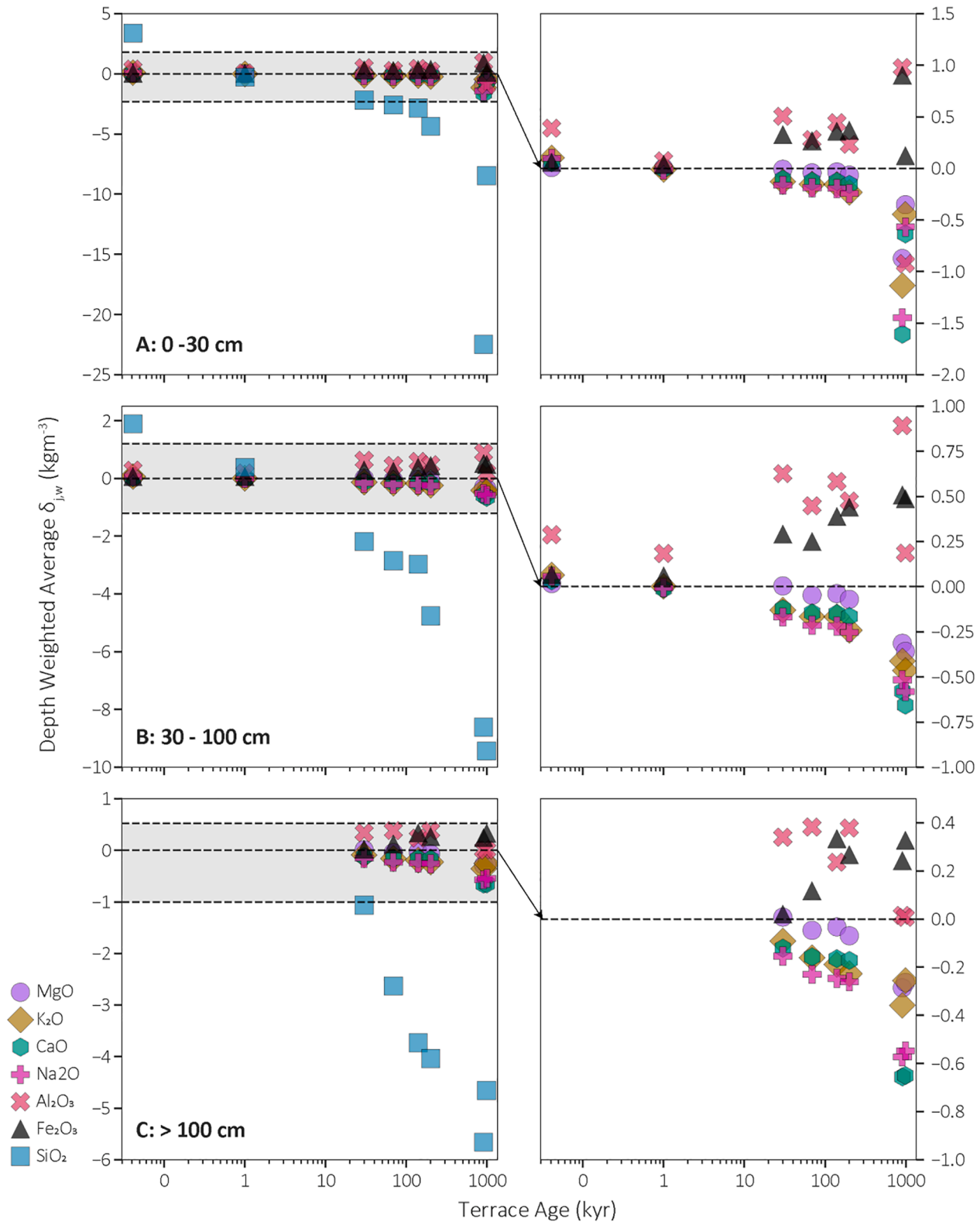

Fig. 2. Depth weighted $\delta_{j,w}$ (kgm^{-3}) for soil depth intervals 0–30 cm, 30–100 cm and below 100 cm. Left column - depth weighted mass change for Mg, K, Ca, Na, Al, Fe and Si. There is Si loss with age for all depth intervals. Right column – zoomed in depth weighted mass change for Mg, K, Ca, Na, Al, and Fe. There is Al and Fe enrichment and Mg, K, Ca, and Na depletion with age for all depth intervals.

associations, which provides chemical protection from decomposition through the adsorption of OM onto mineral surfaces. This chemical protection is conducive to longer mean residences times of 10 to 1,000 of years compared to the particulate organic carbon (POC) fraction which is either free floating or physically protected through occlusion in aggregates (Blanco-Canqui and Lal, 2004; Rasmussen et al., 2005; Totsche et al., 2018), (Lavallee et al., 2020; Lehmann and Kleber, 2015). However, a myriad of studies have found that it is not only texture, but

Table 2
Terrace soil organic carbon (SOC) stocks (kg m2) for total profile and each depth interval.

		SOC Stock (kg m^2)			
Terrace	Age (kyr)	0–30 cm	30–100 cm	>100 cm	Total
T1a	0.041	1.97	0.69	0.00	2.66
T1b	1	3.45	3.33	0.00	6.78
T2	30	14.27	11.16	3.21	28.65
T3	69	11.16	4.51	4.43	20.09
T4	140	4.88	5.92	5.01	15.81
T5	200	11.57	10.00	7.76	29.32
T6	908	8.04	7.85	15.24	31.12
T7	990	11.06	7.84	13.09	31.99

Table 3
R-squared values for SOC density (kg m^{-3}) and variables with analysis for all samples and subsets of samples for intervals 0–30, 30–100, and >100 cm.

	Full Profile	0–30 cm	30–100 cm	> 100 cm
Age (kyr)	0.009	0.052	0.026	0.066
CEC (cmolc kg^{-1})	0.663	0.794	0.699	0.000
Ald (g kg^{-1})	0.517	0.588	0.300	0.578
Alo (g kg^{-1})	0.590	0.604	0.398	0.331
Alp (g kg^{-1})	0.728	0.581	0.531	0.281
Fed (g kg^{-1})	0.000	0.194	0.011	0.018
Fep (g kg^{-1})	0.832	0.712	0.677	0.156
Feo (g kg^{-1})	0.494	0.404	0.314	0.158
0.5 × Feo + Alo (g kg^{-1})	0.607	0.584	0.408	0.364
Sand %	0.034	0.197	0.078	0.260
Silt %	0.047	0.464	0.340	0.194
Clay %	0.010	0.024	0.006	0.440
Center Depth (cm)	0.243	0.143	0.326	0.358
pH	0.000	0.312	0.082	0.075
SOC %	0.945	0.918	0.964	0.978

mineral composition as well that influences how well a clay or silt size particle will protect SOC (Rasmussen et al., 2018). Specifically, poorly crystalline minerals (PCMs) containing Fe and Al have been shown to have a strong positive association with SOC content (Lawrence et al., 2015; Masiello et al., 2004). As such, understanding how the abundance of PCMs evolves in the critical zone (CZ) is important for SOC prediction and modeling (Slessarev et al., 2022).

During pedogenesis Al rich minerals, such as feldspars, and Fe-bearing primary minerals, such as biotite and magnetite, weather and alter to form nanocrystalline hydroxide-rich secondary minerals that then slowly polymerize through dehydration to form stable crystalline secondary minerals. Poorly crystalline Fe-oxides are composed of crystallites of ferrihydrite or nano-goethite and Al-hydroxides and oxyhydroxides, are composed of crystallites of allophane, imogolite, and halloysite. Due to their nano-crystalline structure, PCMs have extremely high surface area and a mix of charges that are conducive to creating organo-mineral associations that protect OM organic matter from microbial decomposition (Eusterhues et al., 2003; Kaiser and Guggenberger, 2003; Kleber et al., 2015; Lawrence et al., 2021; Mikutta et al., 2005; Mudd and Yoo, 2010; Parfitt and Childs, 1988; Yoo and Jelinski, 2016). Although PCMs may make up a small fraction of the total mineral content of the soil, this fraction can account for a disproportionate amount of the total SOC storage. For example, across a chronosequence (300 yr to 4,100 kyr) of volcanic soils on the Island of Hawaii, Torn et al. (1997) found that organic matter sorbed to non-crystalline clays accounted for >40% of OC content variation in all mineral horizons. However, over long timescales PCMs are metastable and weather to more crystalline Fe and Al bearing clays, such as goethite or kaolinite respectively, which have lower surface area and less reactive surfaces to bond with OM (Chorover et al., 2004; Garcia Arredondo et al., 2019; Masiello et al., 2004; Torn et al., 1997). Torn et al. 1997 documented this shift when they saw a peak in PCMs and SOC on 150 kyr lava flows and an increase in crystalline forms accompanied by a drop in SOC stocks for older surfaces approaching 1 Ma. Analysis of OM association with PCM at depth is important to characterize because the abundance of PCMs is variable with depth as well as with age.

Historically, most studies focus on SOC measurements in the top 30 cm (Yost and Hartemink, 2020), where the highest density of SOC is typically observed. However, a growing number of studies highlight the significant contribution of "deep" SOC stocks in many landscapes (Fontaine et al., 2007; Harper and Tibbett, 2013; Jobbágy and Jackson, 2000; Moreland et al., 2021). Fluxes of OM decrease with depth, contributing to observed rapid decline in SOC content in deeper soil horizons. Nevertheless, microbial activity, root exudates, and infiltration of dissolved organic carbon (DOC) supply deep regolith with OM (Guggenberger and Kaiser, 2003; Kaiser and Kalbitz, 2012; Sanderman et al., 2008; Sanderman and Amundson, 2008). SOC in deep horizons are sometimes considered to be "recalcitrant" with limited ability to be degraded by microbes (Rumpel and Kögel-Knabner, 2011), but potential turnover and accessibility may be greater than previously thought. While most studies of deep SOC have been conducted on landforms underlain by thick unconsolidated deposits, the potential for SOC storage in weathered bedrock must be evaluated (Harper and Tibbett, 2013; Lal, 2018; Moreland et al., 2021; Riebe et al., 2017; Georgiou et al., 2022). For example, Moreland et al. (2021) found on average that 74% of OC was located below the A horizon and that up to 30% was stored in saprolite, material where original rock fabric is maintained but weathering has increased friability and porosity (Graham et al., 2010) across a bio-climosequence in the Sierra Nevada, California. Work by Riebe et al. (2017) focused on deciphering the range of mechanisms that may control the penetration depth of the critical zone into bedrock. These deep CZ forming mechanisms have not been applied to consider their influence on SOC stocks. As a result, factors operating over a range of scales such as tectonic stresses, frost weathering (Marshall et al., 2015), and groundwater dynamics (Rempe and Dietrich, 2014), which have been proposed to set critical zone depth, may play a role in determining the depth, magnitude, and stability of SOC stocks.

Here, we synthesize previous data and analyses (Almond et al., 2007; Lindeburg et al., 2013) with new analysis of the Siuslaw River Chronosequence (SRC) soils from terraces in the Oregon Coast Range (OCR) to quantify what controls SOC density, total SOC storage, and the timescales and depths at which controlling variables are significant. We perform a geochemical mass balance, analyze total soil organic carbon stocks, and connect geochemical and physical properties to SOC content to advance our understanding of how weathering alters mineral assemblages, thus soil geochemistry, and influences SOC storage. We partition our analysis into three depth intervals: 0–30, 30–100, and >100 cm, in addition to an analysis of full soil profiles to parse out variable controls on SOC storage with soil development. We also use the chronosequence to analyze the timescales of PCM production and subsequent conversion to more crystalline Fe and Al forms and their accompanying association with SOC. Specifically, we seek to determine if a "sweet spot" or peak of PCM concentration is observed along the SRC, and if an associated peak in SOC storage is present, as has been observed in a limited number of studies conducted in settings with volcanic substrate (Lawrence et al., 2015; Torn et al., 1997). Further, determining the timescales of weathering products that regulate SOC storage could motivate efforts to couple geomorphic, geochemical, and biological models for land management practices that optimize SOC storage.

2. Materials and methods

2.1. Study Region: Oregon Coast range

Hillslopes in the Oregon Coast Range are soil mantled and tend to be steep and highly dissected with relatively uniform ridge and valley terrain that is sculpted by shallow landslides, debris flows, and fluvial

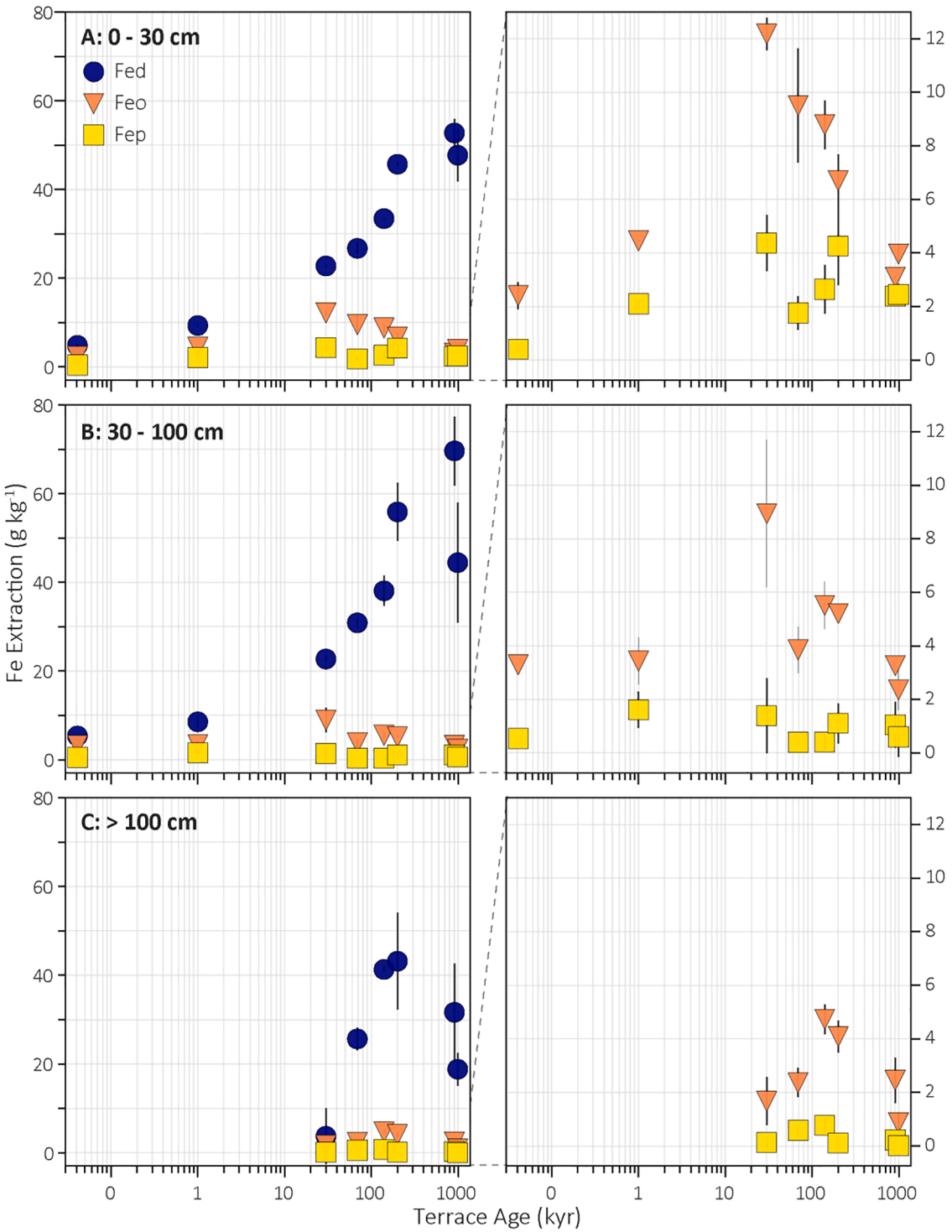

Fig. 3. Depth weighted averages over time for the dithionite-citrate-bicarbonate (Fed - blue circle), oxalate (Feo - orange triangle), and sodium pyrophosphate (Fep - yellow square) extractions for depth intervals 0–30 **(A)**, 30–100 (**B**), and >100 cm (**C**). Fed, a proxy for crystalline Fe forms, increases with terrace age reaching a maximum at 990 kyr in the 30–100 cm interval. Poorly crystalline minerals (PCMs), approximated by Feo, and organo-metal complexes (Fep) are emphasized in the right column. PCMs peak in both the 0–30 and 30–100 cm intervals at 30 kyr, then decline with terrace age. Error bars represent the standard deviations of measured values in the interval.

incision (Dietrich and Dunne, 1978; Montgomery, 2001; Reneau and Dietrich, 1991). Much of western Oregon is underlain by a thick sequence of Eocene sedimentary rocks that include the Tyee Formation, a sand-rich sequence of turbidite deposits (Chan and Dott, Jr., 1983; Heller and Dickinson, 1985; Lovell, 1969) that overlie volcanic basement rocks associated with Siletzia (Wells et al., 2014, 1998; Wells and Heller, 1988; Wells and McCaffrey, 2013). Long-term rock uplift rates measured via marine terraces vary from <0.1 to 0.3 mm yr^{-1} in the region (Beschta, 1978; Kelsey et al., 1996), which are similar to erosion rates measured by cosmogenic radionuclides and suspended sediment records of 0.06 to 0.15 mm yr^{-1} (Heimsath et al., 2001; Marshall et al., 2017; Penserini et al., 2017; Reneau and Dietrich, 1991). In general, long-term uplift rates are lower than geodetic uplift rates, reflecting the earthquake deformation cycle (Mitchell et al., 1994).

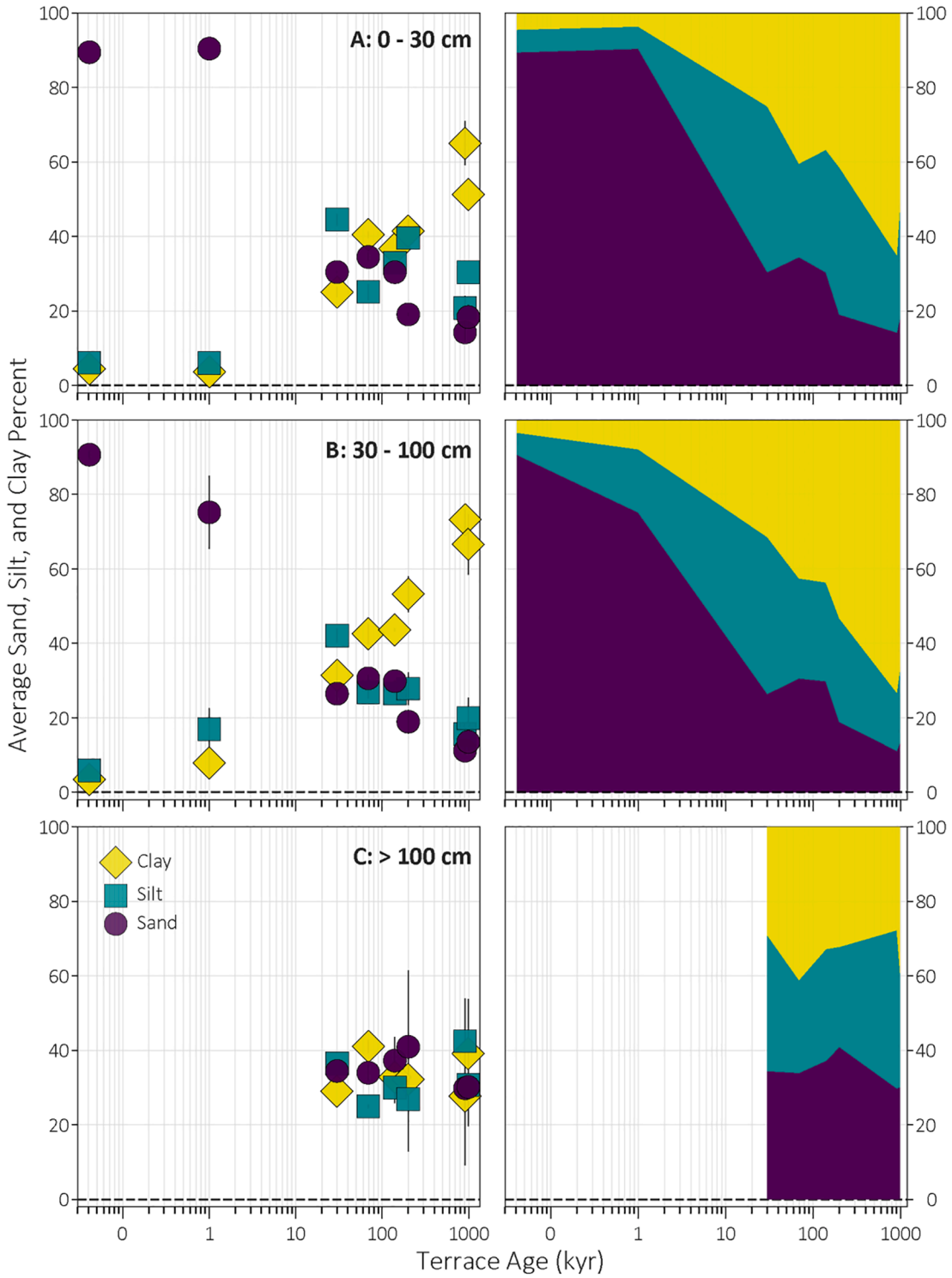

Fig. 4. Depth weighted averages over time for clay (yellow diamond), silt (green square), and sand (purple circle) percent depth intervals 0–30 (A), 30–100 (B), and >100 cm (C). Young soils are dominated by sand until ~30 kyr where clay percent is the highest. Silt increases with clay until ~30 kyr where it begins to decline.

The region is characterized by a Mediterranean climate with warm summers with minimal precipitation and wet and cool conditions in the winter (Patching, 1987). Western OCR has a mean annual average temperature (MAAT) of 10–11.1 ℃ and mean annual precipitation (MAP) between 1,800–2,600 mm respectively with most occurring between fall and spring. The dominant vegetation is coniferous trees, particularly Douglas fir [*Pseudotsuga menziesii* (Mirbel) Franco] and Western hemlock [*Tsuga heterophylla* (Raf.) Sarg.] Subdominant and less abundant species include Sitka spruce [*Picea sitchensis* (Bong.) Carr.] and Western red cedar [*Thuja plicata* (Donn) ex D. Don]. The understory in the region hosts salal (*Gaultheria shallon* Pursh), salmonberry (*Rubus spectabilis* Pursh), and evergreen huckleberry (*Vaccinium ovatum* Pursh) (Patching, 1987). Widespread fire management by indigenous peoples as well as stand-replacing fires have been documented historically and lake cores reveal Holocene fire return intervals of 200–300 years (Gavin et al., 2003; Long et al., 1998). More recently, the region has been subject to widespread timber harvest activity for the past 80–100 years.

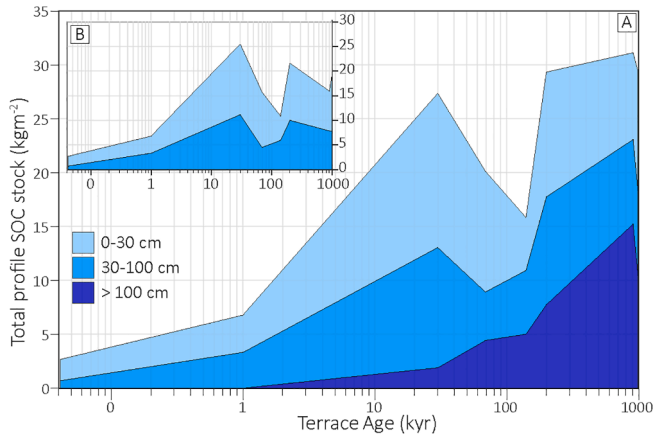

Fig. 5. Total SOC stock (kgm^{-2}) for each terrace. Light blue represents SOC stored in the top 30 cm of each profile, blue is SOC in 30–100 cm, and dark blue is SOC stored below 100 cm. SOC in the top 30 cm dominates younger terraces, but as soil age increases (and soil depth increases), SOC stored below 100 cm begins to play a larger role. In T6 (908 kyr) about 48% of total SOC is stored below 100 cm. SOC stock below 100 cm is removed in inset A. When SOC >100 cm is excluded, SOC stock peaks around 30 kyr, but then declines with age, which demonstrates the significance of SOC below 100 cm.

2.2. Siuslaw River soil chronosequence

Almond et al. (2007) identified and analyzed soils from the Siuslaw River Chronosequence (SRC) that consists of 7 distinct surfaces created by fluvial incision (T1-T7; Fig. 1). These terraces were carved by progressive lateral migration of a large bedrock meander in the Siuslaw River in the central section of the OCR. T1-T5 were sampled until auger refusal, coincident with unweathered bedrock. Sampling on T6 and T7 was limited by the practicalities of hand augering to 9 and 10 m, respectively (for more details on sample collection see Almond et al., 2007). In almost all cases, surfaces are strath terraces which are characterized by 1 to 2 m of fluvial sediment over beveled bedrock. The lowest terrace (T1) is the exception, which includes >2 m of overbank sediment with intercalated buried soils. The first five fluvial terraces (T1-T5) narrow as they increase in elevation and age. The oldest terraces (T6 and T7) are narrow but well-defined surfaces that are remnants of much more extensive surfaces that have been truncated by progressive uplift and erosion of the ridge defined by the meander (Fig. 1).

Terrace ages for T1 and T2 were determined by radiocarbon dating while ages for T3 to T7 were derived from an incision rate of 0.18 ± 0.04 mm yr^{-1} and elevation above modern channel (further details on dating methods found in Almond et al., 2007). For the purposes of this study, we separated the soil of T1 into 4 units (T1a – T1d) corresponding to 3 individual buried soils and a capping flood deposit associated with a regionally significant flood in 1964 (Harr, 1981). We limited our analysis from the top two: T1a and T1b (Appendix Fig. A1). T1a, classified as an Entisol by Almond et al. (2007), consists of sandy and relatively unweathered material reflecting historic deposition and minimal alteration, overlain by a 10 cm thick A horizon. T2 is characteristic of an Inceptisol with a thick A horizon as well.We applied an age of 41 years to T1a determined by the time between sample collection (2005) and flood (1964). For T1b, the youngest of the buried soils in T1, we interpolated an age of 1 kyr +/- 500 yrs, with the assumption it is younger than the oldest buried soil where radiocarbon dates of material at the base suggest 3.5 kyr (Table 1). Observations from Almond et al 2007 demonstrate unisequal pedogenic development as T2 to T5 progress from an Inceptisol to Alfisol to an Ultisol. Both T6 and T7 are classified as Ultisols as well.

Almond et al. (2007) calibrated a soil chronofunction for the SRC that connects the rubification of soils to soil properties and age (Sweeney et al., 2012). They demonstrated that mean soil residence time varies locally by orders of magnitude in response to stream capture, deep-seated landsliding, and lateral channel migration. Lindeburg et al. (2013) furthered this analysis and explored the curious lack of podsolization in the Siuslaw chronosequence, which contrasts with marine terraces found at similar latitude along Oregon Coast, with detailed soil chemical, physical and mineralogical analysis of the SRC soils. The authors postulate that lithology, vegetation or climate alone do not control this and could be the result of multiple combined factors. Such as, dryer inland soils, higher pH in surface soils, and more rapid increase in clays in the inland fluvial SRC chronosequence. Their measurements included OC content, soil texture, pH, geochemistry, mineralogy, and conducted iron and aluminum extractions across age and depth. They observed an increase in Al and Fe with age that supports the rubification of soils. Here we expand upon Lindeburg et al. (2013) SOC analysis to include soil depths >1 m and analyze the controls of SOC density with age and depth and the connections to Al and Fe mineral evolution with soil development.

2.3. Elemental mass change calculations

We characterized how weathering altered the chronosequence soils and their affinity for organic matter through time through changes in soil geochemistry. Major element concentrations were measured for Mg, K, Ca, Na, Al, Fe, and Si by X-ray fluorescence (XRF) at ALS Minerals, Reno, NV. We calculated absolute mass changes of a specific element *j* in weathered material *w,* ($m_{j,flux}$), per unit volume of parent rock V_p according to the following mass balance formulation (Anderson et al., 2002; Brimhall et al., 1991; Brimhall and Dietrich, 1987; Chadwick et al., 1990):

$$\delta_{j,w} = \frac{m_{j,flux}}{V_p} = \frac{1}{100}\left(C_{j,w}\rho_p\frac{C_{i,p}}{C_{i,w}} - \rho_p C_{j,p}\right) \quad (1)$$

where C_j is the concentration in weight percent of element *j*, ρ [ML^{-3}] is the bulk density, m_j is the mass flux of element *j*. The subscript *i* refers to an immobile element. We use Zr as our reference immobile element and alluvium for the reference parent material for T1-T5 and unweathered bedrock for T6 and T7. Negative $\delta_{j,w}$ values indicate elemental loss and positive values represent accumulation or gain. To identify the variable timescales of weathering and elemental changes with soil development, we calculated depth weighted $\delta_{j,w}$ averages for the soil intervals 0–30, 30–100, and >100 cm (Fig. 2).

2.4. Organic carbon calculations

Lindeburg et al. (2013) measured organic carbon (OC) of the fine fraction soil (<2 mm). From their measured SOC% values (see Table A.1 for values), we calculated SOC density as a mass per volume [ML^{-3}]. For each interval of soil depth sampled and analyzed, we calculate *SOC density* in within a horizon as:

$$SOC\ density = 0.01 \cdot \%SOC \cdot \rho_{n,\,total} \quad (2)$$

where ($\rho_{n,total}$) is dry total bulk density [ML^{-3}]. Coarse material (>2 mm) was negligible for all sites, besides on horizon in T4 where evidence of a potential debris flow deposit exists at depth (Almond et al., 2007), thus we do not incorporate a coarse fraction correction into our bulk density calculations. This could result in a slight overestimation of SOC density for that soil depth at T4.

We calculated SOC stock [kgC m^{-2}] for each soil horizon by multiplying the horizon *SOC density* and the horizon thickness (*h*) [L], then summing all soil horizon SOC stock values in the profile (Table 2). Additionally, we calculated the SOC stock for depth intervals; 0–30, 30–100, and >100 cm to determine how soil depth modulates the interplay between measured soil properties and *SOC density* (see Table 3).

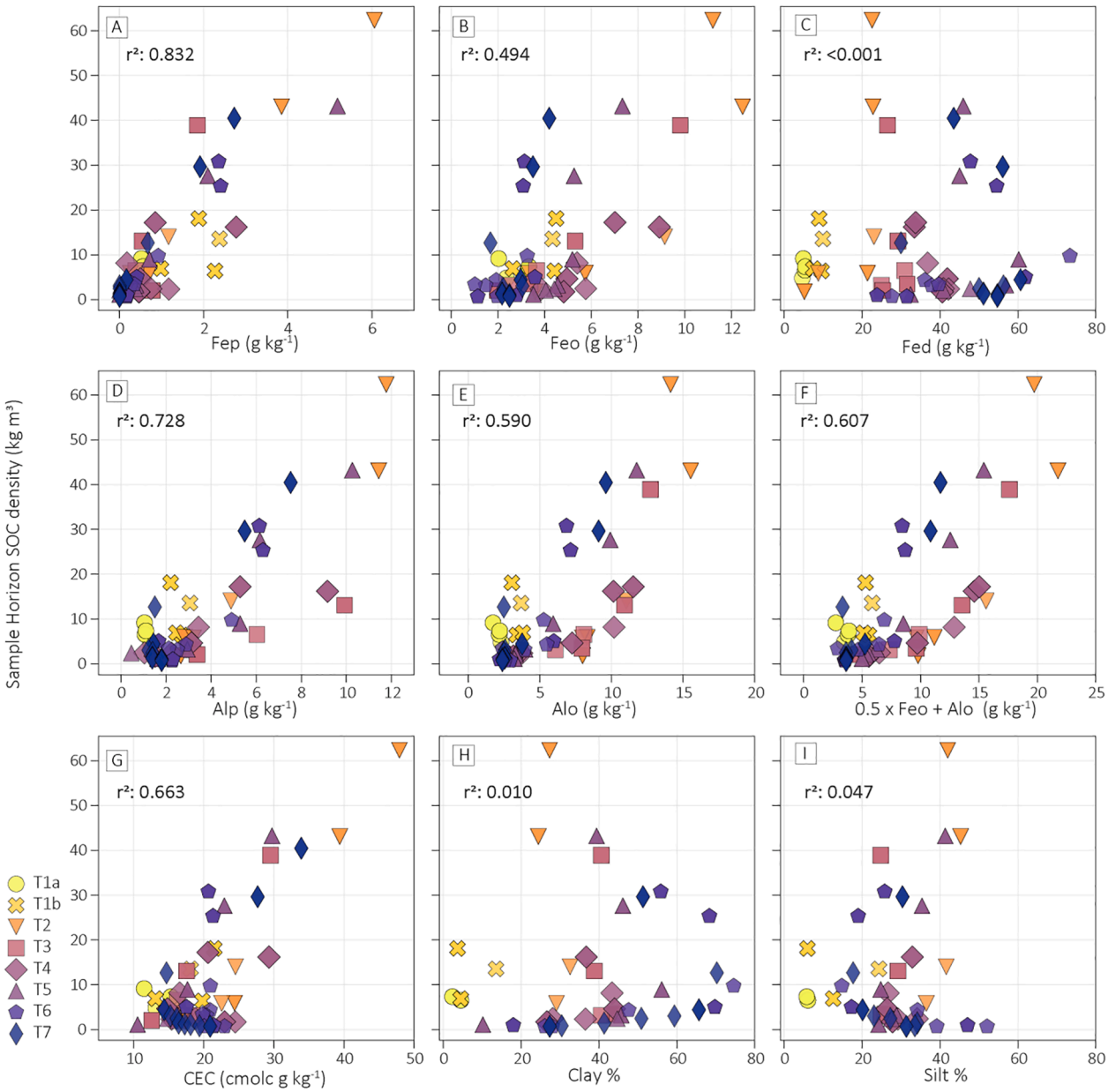

Fig. 6. SOC density (kgm^{-3}) from all terraces and soil layers where data was measured versus A) Fep (g kg^{-1}), B) Feo (g kg^{-1}), C) Fed (g kg^{-1}), D) Alp (g kg^{-1}), E) Alo (g kg^{-1}), F) Alo + 0.5 Feo (g kg^{-1}), G) CEC (cmolc kg^{-1}), H) Clay %, I) Silt %.

2.5. Iron extractions

We characterize the evolution of organo-metal complexes, PCM, and crystalline pedogenic mineral concentrations and how they relate to SOC content by correlating previously measured and published concentrations of three Fe and two Al extractable fractions conducted by Lindeburg et al. (2013) to SOC density measurements. Lindeburg et al. (2013) conducted three separate extractions in parallel; 1) sodium pyrophosphate (Alp and Fep), which is expected to reflect the organically complexed metals (McKeague, 1967), 2) ammonium acid oxalic acid buffered at pH 3 (Alo and Feo) which is expected to isolate PCMs in addition to phases extracted by Alp and Fep, such as ferrihydrite and nano-crystalline goethite (McKeague and Day, 1966), and 3) dithionite-citrate-bicarbonate extraction of Fe (Fed) is expected to extract crystalline Fe forms in addition to phases extracted by oxalate and pyrophosphate extractions (Mehra and Jackson, 1958). Since Fe and Al extractions were done in parallel, thus some overlap between extractions is expected. Lindeburg et al. (2013) reported a <6% variation analytical replicates of pedogenic oxide measurements. To show trends with soil age and depth, we calculated a depth-weighted average for each extraction. Additionally, we approximated short-range order mineral concentration by calculating Alo + 0.5Feo (Lindeburg et al., 2013). We present the depth variability of measurements used to calculate the depth weighted average within a depth interval by standard deviation of the soil horizon measurements within each 0–30, 30–100, and >100 cm interval (Table B.1 and C.1 for Fe and Al respectively).

2.6. Statistical correlation analyses

We used open-source packages in Python to calculate correlation coefficients (Tables D.1-4) and r^2 values between SOC density, OC%, terrace age, Fe and Al extractions, texture, pH and cation exchange capacity (CEC). We conducted this analysis for all layers in the whole profile as well as for each depth interval. We adjusted the depths in T1b, so that the top of the buried soil (bottom of T1a) is 0 cm for T1b.

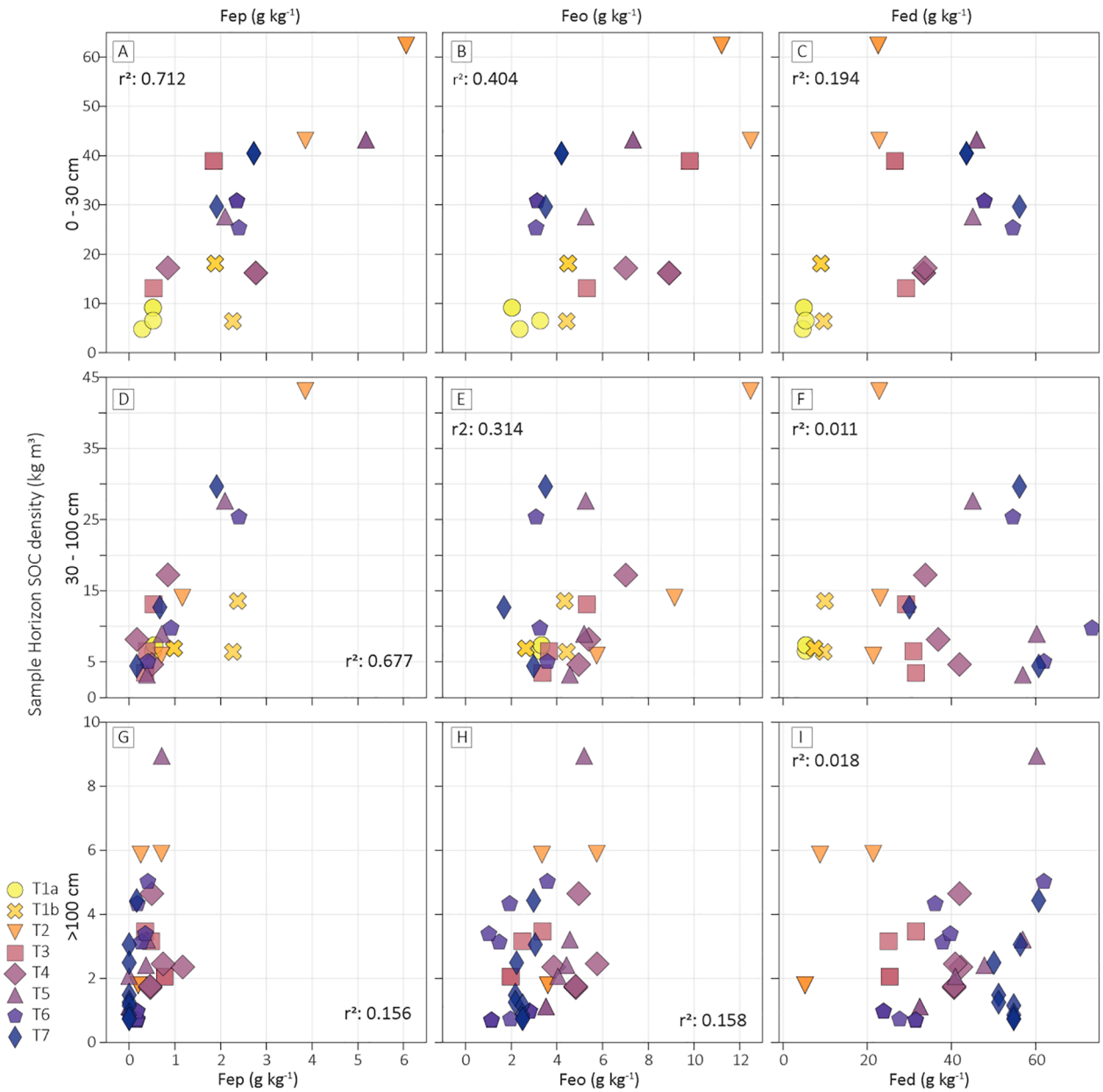

Fig. 7. SOC density (kg m^{-3}) vs Fep (g kg^{-1}) (A, D, and G), Feo (g kg^{-1}) (B, E, and H), and Fed (g kg^{-1}) (C, F, and I) extractions from all terraces and soil layers for soil intervals 0–30 (A-C), 30–100 (D-F), and >100 cm (G-I).

3. Results

3.1. Elemental mass change

As soils age, they become relatively enriched in elements associated with secondary pedogenic minerals, particularly Fe and Al (Fig. 2a). For each depth interval, we observe a loss of more soluble elements, such as SiO_2 and CaO, as terraces age. Our data show the greatest total mass loss of SiO_2, due to high concentrations in the parent material. Although less pronounced on a mass basis, our data also show loss of MgO, K_2O, CaO, and Na_2O with soil age. These results are consistent with other studies that examined elemental loss with continual soil weathering (Anderson et al., 2002). Al_2O_3 and Fe_2O_3 are the only two elements to be enriched, with Fe experiencing an age-related increase in elemental mass. An exception is present for Al, where Al is lost in the >100 cm depth interval for T6 and T7.

3.2. Fe and Al extractions

Progressive weathering and soil development is visible in the Fe and Al extraction data. The increasing formation of crystalline pedogenic Fe mineral forms is shown by the increase of the depth weighted average of Fed with terrace age (Fig. 3). This is true for all three depth intervals, with the highest Fed concentration, 69.64 +/-7.75 g kg^{-1} in the 30–100 cm interval of T6. There is a peak in depth-weighted average of 12.18 +/- 0.60 g kg^{-1} Feo, approximating PCMs, at 30 to 69 kyr in the top 0–30 cm. A smaller less pronounced peak ~4.37 +/- 1.04 g kg^{-1} occurs for the average Fep, approximating the organo-metallic complexes. However, there is greater overlap in the Fep measurements, shown by standard deviations of measurements in that interval (black lines through data). Since PCM content varies with depth standard deviations of measurements within depth intervals are expected. In the 30–100 cm interval, we observe a small peak in Feo at 30 kyr with 8.94 +/- 2.75 g kg^{-1}. Fep abundance is minimal in the >100 cm interval for all ages. As

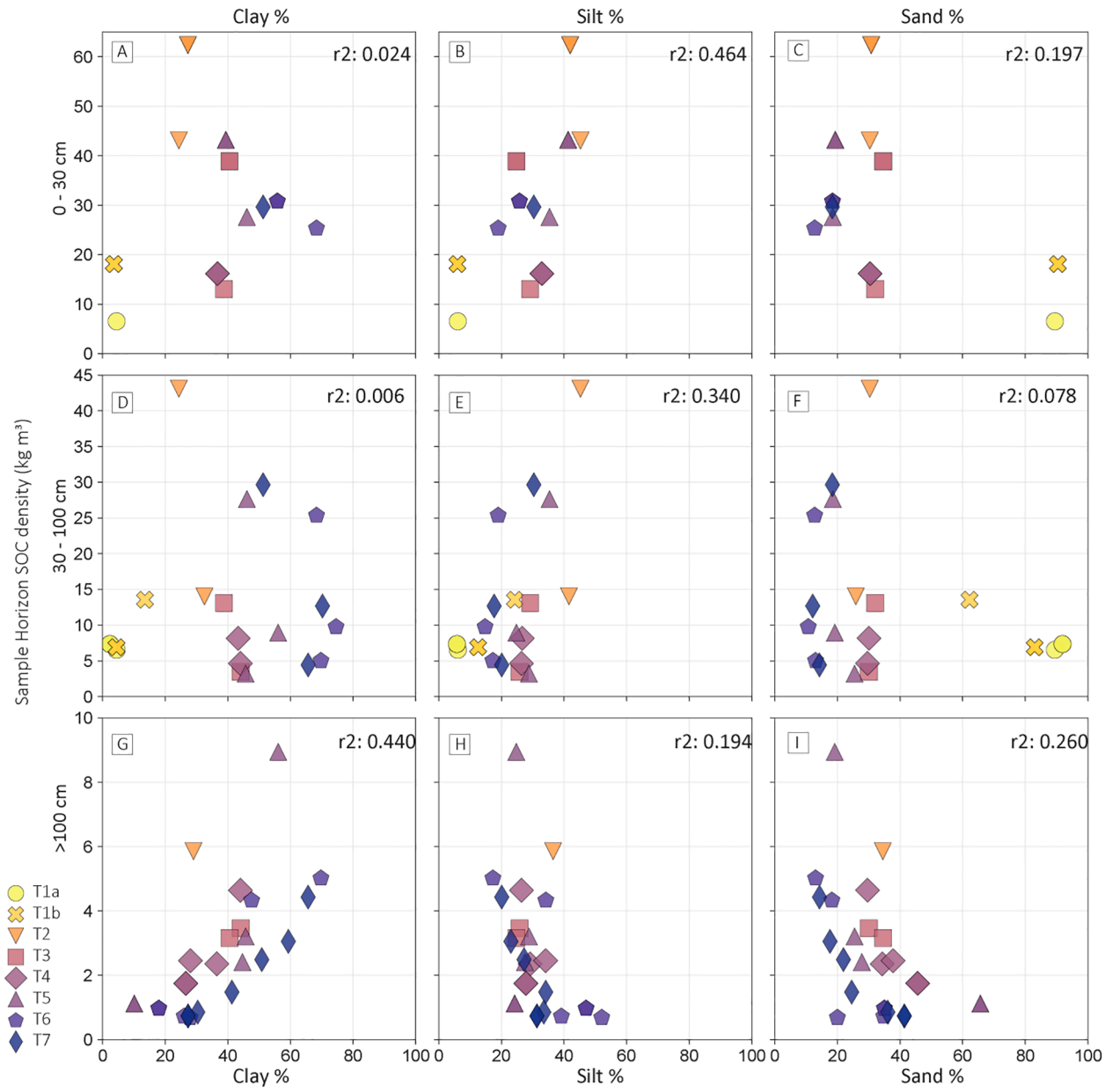

Fig. 8. SOC density (kg m^{-3}) vs clay % (A, D, and G), silt % (B, E, and H), and sand % (C, F, and I) extractions from all terraces and soil layers for soil intervals 0–30 (A-C), 30–100 (D-F), and >100 cm (G-I).

soils get older the fraction of total crystalline minerals (Fed) becomes dominant.

Oxalate and pyrophosphate extractable aluminum (Alo and Alp respectively) follow similar trends as Fe with time (Appendix Fig. B1). Alo and Alp both peak ~30 to 69 kyr with concentrations of 15.20 +/- 0.56 g kg^{-1} and 11.50 +/- 0.16 g kg^{-1} respectively in the top 30 cm. There are less pronounced peaks in the 30 – 100 cm interval (11.08 +/- 2.98 g kg^{-1} and 5.27 +/- 3.675 g kg^{-1} respectively) and overlap of standard deviations of measurements. Below 100 cm a peak in Alo exists, but there are few measurements in this horizon and overlap in values between terraces exists.

3.3. Texture evolution

Soils become increasingly finer textured with terrace age due to increased exposure time to weathering. Young soils dominated by sand with T1a –T2 being >80% sand (Fig. 4). In the 0–30 and 30–100 cm intervals, the average clay and silt percent values increase at a similar rate as sand declines until 30 to 69 kyr. Silt percent declines in soils >30 kyr, while clay continues to increase making up >60% of the soil in the top 100 cm for the oldest terraces, as shown by the top yellow fraction in Fig. 4 stack plots. In the >100 cm depth interval, the shift from sand to clay rich soils is less pronounced. Clay increases from ~25% to ~40% while sand experiences a decline in that range.

3.4. Total soil organic carbon stocks

Total SOC stock is low in the youngest soils (<5 kg m^{-2}) and reaches a maximum in T7 with ~32 kg m^{-2} (Fig. 5 and Table A.1). Prior to 30 kyr, soils are <100 cm thick and SOC stock in the top 30 cm makes up >50% for T1a and T1b (~73% and ~51% respectively). In addition to having shallower depths, thus less vertical space to accommodate SOC, T1a and T1b also have the lowest SOC content across all soil depths (Appendix Fig. C.1), resulting in lower total stocks when integrated with depth. Total SOC stock in the top 100 cm, dips between 30 and 69 kyr (Fig. 5. inset A) but increases again after 120 kyr. Consistent with other

studies and expectations, SOC density and concentration decline with depth. Although SOC density is low below 100 cm, the SOC stored at these depths becomes a significant contributor to total SOC constituting ~48% of the total SOC stock in the 908 kyr and ~40% in 990 kyr.

3.5. Soil organic carbon density and geochemical and physical soil properties

We correlated geochemical and physical soil properties to SOC density values for all samples (from all depths and terrace ages) (Fig. 6). In line with previous studies (Lawrence et al., 2015; Masiello et al., 2004), both Alp and Fep had a positive correlation, $r^2 = 0.728$ and 0.832 respectively (Table 2) with SOC density regardless of terrace age (Fig. 6a and d). Alo and Feo, which extract PCM material in addition to the organo-mineral complexes extracted with the pyrophosphate extraction, are also positively correlated with SOC density ($r^2 = 0.590$ and 0. 494 respectively) (Fig. 6b and e). Terrace age appears to modify the slope of the Feo relationship with SOC, where SOC is more sensitive to Feo (i.e., steeper slope on the graph) for older terraces. This is not as prominent for the SOC density relationship with Alo. Fed, which also includes crystalline forms of pedogenic Fe minerals, does not have a clear relationship with SOC density when analyzing samples from all depths and terraces ($r^2 = <0.001$) (Fig. 6c). However, the overall increase of Fed with terrace age is evident, which is consistent with the increasing crystallinity expected with soil age. It is also evident that clay content also increases with age, but there is not a corresponding increase in SOC density ($r^2 = 0.010$) when looking at samples from all depths and terraces (Fig. 6h).

3.5.1. Soil depth intervals: Fe and al extractions

The relationship between SOC density and Fe and Al extractions varies with depth and extraction type. In the top 30 cm, SOC density increases with Fep ($r^2 = 0.712$) and Feo ($r^2 = 0.404$) concentration (Fig. 7a-c). Although SOC density increases with Feo in the top 30 cm, T1a and T1b have the lowest concentration in both SOC and Feo, which both increase for T2 – T4. However, in the oldest three terraces (T5-T7) both SOC and Feo concentrations decline. Fed increases with terrace age, but SOC does not increase consistently in a similar fashion. There is an increase in SOC density in T2 that declines at T3-T4, then increases slightly for T6 and T7. In the 30–100 cm interval, Fep concentrations are lower, but a positive relationship with SOC persists ($r^2 = 0.677$) (Fig. 7d). SOC does not increase consistently with Fed in the 30–100 cm interval ($r = 0.013$), but again an increase in Fed with terrace age exists. Below 100 cm, SOC does not vary systematically with Fep ($r^2 = 0.156$), Feo, ($r^2 = 0.158$), or Fed ($r^2 = 0.018$) (Fig. 7g - i), likely owing to very low concentrations of Fep and Feo, as well as low OM input at these depths.

With depth, Alp and Alo follow similar trends as Fep and Feo (Appendix Fig. D.1). In the top 30 cm SOC density increases with both Alp ($r = 0$ 0.581) and Alo ($r = 0$ 0.604). With increasing depth, Alp and Alo concentrations become less correlated with SOC density. Alp and Alo concentrations in the 30–100 cm layer are lower (<15 g kg^{-1}) as well as the >100 cm interval (<4 and 10 g kg^{-1} respectively).

3.5.2. Soil depth intervals: Texture

Younger terraces have greater sand content and lower SOC concentration compared to older terraces dominated by clay and silt. Our data show that as soils age, sand content decreases as weathering produces more silt and clay sized minerals. Within the whole profile, SOC density is negatively correlated with sand, while increasing with higher silt content and clay. Notably, in the top 30 cm, clay content increases with terrace age (Fig. 8a), but SOC is not strongly correlated to this increase ($r^2 = 0.024$). On the other hand, SOC density does have a slight positive correlation with silt ($r^2 = 0.464$) and weak negative correlation with sand in the top 30 cm ($r^2 = 0.197$) (Fig. 8b, c). Clay content also increases with terrace age in the 30–100 cm interval, but there is no corresponding SOC density increase ($r^2 = 0.006$) (Fig. 8 d). Sand decreases with terrace age, but there is not a strong correlation with SOC ($r^2 = 0.034$) (Fig. 8 e).. Below 100 cm, SOC density increases with clay content ($r^2 = 0.440$) (Fig. 8g).

4. Discussion

4.1. Siuslaw River chronosequence development and controls on soil organic carbon

Our analysis of how geochemical characteristics, physical properties, and SOC content vary with age and depth demonstrates the key role weathering plays in SOC storage and distribution (Fig. 9). Young soils in the SRC, underlain by sandstone and mudstone, are dominated by coarse, relatively unweathered material made up of sand-sized mineral grains dominated by feldspars. As soils in the SRC age, older soils are enriched in quartz as plagioclase and potassium feldspars weather to secondary clay minerals (Lindeburg et al., 2013). This increasing degree of weathering with soil age is supported by the production of clay sized minerals, enrichment in Fe- and Al- bearing pedogenic products and depletion of elements like Si as leaching takes place (Fig. 2). These results complement the rubification of soils characterized in Almond et al. (2007) and the weathering patterns of the SRC reported in Lindeburg et al. (2013).

The progressive accumulation of Al and Fe, the loss of highly mobile cations and other elements, as well as the increase in clay alone are not effective predictors of the controls on SOC accumulation and stabilization. Rather the mineral-specific weathering pathways provide key explanation as to where and how SOC is stored in soils and what processes are critical for soils of different ages. Specifically, the evolution of organo-metal complexes, poorly or nano-crystalline oxide minerals, and crystalline oxide phases strongly correlates with SOC storage across the SRC (Figs. 6 and 7). Additionally, during this mineralogical evolution, clay content increases - and silt in intermediate ages accompanied by a corresponding decline in sand-sized minerals.

Although SOC increases with both Feo and Fep in the top 30 cm, soil samples cluster by terrace in the top 30 cm along the SOC-Feo and Fep correlations, implying that time-dependent weathering pathways retain a key control on SOC. In contrast, terrace ages do not align with the SOC vs Fep relationship indicating that soil age does not exert a strong control on the correlation of SOC and Fep (Fig. 7a and b). Pyrophosphate extractable Fe and Al, a proxy for organo-metal complexes, are immobile and primarily located in the top 30 cm.

When soils are young, Feo content and SOC density are low, and weathering causes non-crystalline forms to develop resulting in our observed increase in SOC density in the top 30 cm between T2 and T4. When conversion to more crystalline forms occurs, Fed content increases and Feo declines (Fig. 3), but SOC density does not drop to the low values observed for younger soils. This apparent inconsistency is likely due to the fact that as the soils are depleted of PCMs (Feo), crystalline minerals (Fed) and clay content increase which provide large amounts of surface area as well and can form other types of organo-mineral associations that hold onto OC.

When analyzing samples from all ages and depths, SOC is strongly correlated to both non-crystalline Fe extractions - Feo and Fep (Fig. 6) which is consistent with other chronosequence studies (Garcia Arredondo et al., 2019; Lawrence et al., 2015; Mainka et al., 2022; Masiello et al., 2004; Torn et al., 1997). The strength of the SOC relationship with non-crystalline extractions in the SRC, however, decreases with depth. In surface soils (<30 cm), Fep and Feo are strongly correlated with SOC density, but in the 30–100 cm and >100 cm intervals Feo and Fep concentrations decline and the correlation strength with SOC deceases. In the SRC 0–30 and 30–100 cm intervals, both Feo and Fep concentrations peak, particularly Feo, as non-crystalline forms progressively become more crystalline, indicated by an increase in Fed concentrations in soils >30 kyr. A drop in total SOC stock occurs during the 30–69 kyr time interval, as well, and does not recover high values until after 120 kyr (Fig. 5). However, when only examining the top 100 cm, SOC stocks

remain low (Fig. 5 inset) suggesting that the peak observed in non-crystalline minerals may help facilitate a "sweet spot" in SOC storage. This peak in SOC at ~30 kyr is coincident with the peak in non-crystalline Fe and Al fractions and a shift in the dominant texture (Fig. 4). Prior to 30 kyr, sand is the dominant size fraction in the top 100 cm, with silt and clay increasing together at a similar rate. However, for 30–69 kyr soils, clay concentration becomes greater, while sand and silt begin to decline as soils become increasingly weathered.

Although the SRC is underlain by predominantly sandstone and mudstone, our results accord with the conceptual model of Lawrence et al. (2015) developed in volcanic landscapes, which highlights how specific soil properties regulate SOC storage. Their conceptual model suggests that the relevant processes that connect SOC storage and soil properties vary with depth and time. Due to the shallow nature of young soils, the vast majority of the mineral mass is close to the surface and thus likely to interact with OM input and cycling from the surface. On the other hand, although deep soils have more total mineral mass, OM input is limited at depth. This contrast results in thick, highly altered, old soils having a greater proportion of PCM and crystalline minerals compared to young shallow sites, which will have higher fraction of organo-metal complexes.

Lawrence et al. (2015) also reported a peak in SOC stock in shallower soils (<50 cm) for 14 kyr soils in the Cowlitz River Chronosequence, which occurs sooner than the 30 kyr peak we observe in the SRC. However, these chronosequence studies are limited to the ages at which terraces exist and it is promising that our SRC and the Cowlitz data both reveal peak-SOC in shallow soils with ages of the same magnitude (10^4). Nonetheless, the age at which the peaks occur only vary by a factor of 2. This difference could be the result of contrasting parent material and terrace formation. The SRC terraces are formed from deep bedrock weathering (except for T1), while the Cowlitz chronosequence substrate is composed of glacial gravels and outwash sands. The relatively rapid attainment of peak SOC in shallow soils and the slightly higher SOC stocks at the Cowlitz chronosequence could also result from the initial texture, porosity, and other properties of the volcanic parent material. Additionally, the Cowlitz river sediments are likely derived from primarily basalt and andesite gravel with additional mixing of tephra and silt-sized volcanic sediments of the loess input (Lawrence et al., 2015). These materials are ideal for the rapid production of poorly crystalline minerals that are highly effective for bonding with SOC. Additionally climatic differences would also likely influence weathering rates and timescales of SOC accumulation and pedogenic mineral evolution. Lawrence et al. (2021) compared the wetter Mattole River and drier Santa Cruz marine chronosequences and observed that the Santa Cruz chronosequence has lower SOC stocks than the Mattole River. On the Hawaiian basalt flows, SOC in surface horizons (O and A) in Torn et al. (1997) peak around 20 kyr which is similar to the timescale observed for the SRC and the Cowlitz chronosequence.

4.2. Critical zone development and deep soil organic carbon stocks

Although deep carbon has frequently been neglected from prior studies, our findings reveal that nearly all of the total SOC stock is found below 100 cm within the oldest SRC soils. Interest and research in deep soils is increasing, but it is rare to obtain samples from below 100 cm. Deep soil sampling is not frequent practice because OM input and decomposition rates are much slower with depth due to a decline microbial activity and increased protection through processes such as mineral associations and/or aggregate occlusion (Rumpel and Kögel-Knabner, 2011; Schrumpf et al., 2013). Therefore, deep carbon has often been thought of as having a weak influence on total SOC dynamics. Additionally, because sampling is difficult, deep subsoils are often neglected. Particularly in steep, remote terrain, it may be challenging to obtain samples below a certain depth due to the heterogeneity of rocky soils. The common focus on understanding OM dynamics in topsoil has resulted in a knowledge gap in understanding deep carbon dynamics and an underestimation of global SOC stocks (Moreland et al., 2021; Rumpel and Kögel-Knabner, 2011). Additionally, much of the SOC literature has developed through agricultural applications where topsoil characterization is the focus coinciding with the highest concentration and rate of OM cycling. A recent study highlights the tendency to focus on shallow soils and for SOC studies published between 2004 and 2019, the average soil depth measured was 24 cm (Yost and Hartemink, 2020). The lack of understanding of deep SOC dynamics adds to the uncertainty of how soil perturbations (agriculture, wildfire, etc.) will affect SOC stores.

Our results show that weathering and deep SOC are significant contributions to carbon stocks over long time periods. In the SRC, SOC stocks below 100 cm account for 25% of the total stock by 120 kyr, and >40% of the SOC inventory by 908 kyr. Since Feo and Fep are strongly correlated with SOC density and decline with soil age, one might expect a continual decline of total SOC stock as well. However, the non-crystalline phases are concentrated in the top 100 cm. Although we observe a decline in SOC stored in the top 100 cm associated with this mineral control, total organic carbon continues to increase due to the growth of deep carbon stocks. Following the 30 kyr peak in total SOC stock, SOC stock begin to increase again around 120 kyr (T5 – T7) as soil profiles become thick and highly weathered. Although deep SOC concentration (>1 m and up to 6 m) is relative small compared to surface soil, the SOC stock below 1 m can be significant. The timescale at which deep SOC begins to constitute a substantial component of the SOC inventory appears to vary with climate and parent material. Torn et al. (1997) attributed a total SOC stock peak at 157 kyr to a peak in total non-crystalline minerals present in the soil while Lawrence et al. (2015) had a peak in total SOC around 300 kyr, while total SOC storage in the SRC continues to increase even after 908kyr.

After 120 kyr however, these deep stores become increasingly important contributors to total SOC storage. As non-crystalline phases that have large reactive surfaces areas for storing carbon are converted to less reactive lower-surface area crystalline phases with age and weathering, soil depth and clay content increase. Prior to the transition from poorly crystalline sand-dominated soils to crystalline clay-rich soils at 30–69 kyr, SOC below 100 cm was minimal. Although PCMS (approximated by Feo and Alo), which provide strong bonds for OM, decline with terrace age, SOC continues to increase. Larger accommodation space due to increased depth and large clay abundance to be stored at depth with increasing clay abundance and soil thickness. Implying a shift in SOC dependence on PCM phases to clay content and increasing soil depth and mean soil age occurs.

Our results demonstrate that progressive thickening of the weathering zone can facilitate the establishment of substantial SOC stocks, even when SOC concentrations at depth are small (Fig. 5). The spatial and temporal pattern of deep weathering that affects, soil porosity, texture, mineralogy, etc., may result from a variety of mechanisms and Riebe et al. (2017) compares four hypotheses for deep bedrock weathering and critical zone architecture. The combined influence of topographic and tectonic stresses can control the size and location of open fractures in the critical zone that influence fracture flow and exposure to atmospheric and biotic activity critical for soil development (Slim et al., 2015; St. Clair et al., 2015). Another hypothesis for deep CZ development is through a bottom-up control due to the slow drainage of the water table. Draining water allows the drying of rock, creating an oxidizing setting rather than reducing. Additionally, it allows for biotic activity to enter and define the bedrock-soil interface (Rempe and Dietrich, 2014). On the other hand, erosion rates and fluid residence time may control CZ depth through accumulated chemical weathering. The downward advection of reactive water from surface inputs influences mineral weathering and lateral translocation of elements in the soil profile (Lebedeva and Brantley, 2013). This process would influence pH values with depth and thus organo-metal complex formation and percolation into the soil. By contrast, in some regions, frost weathering processes and thus temperature variations may exert a primary role in breaking down bedrock and soil development. (Anderson et al., 2013;

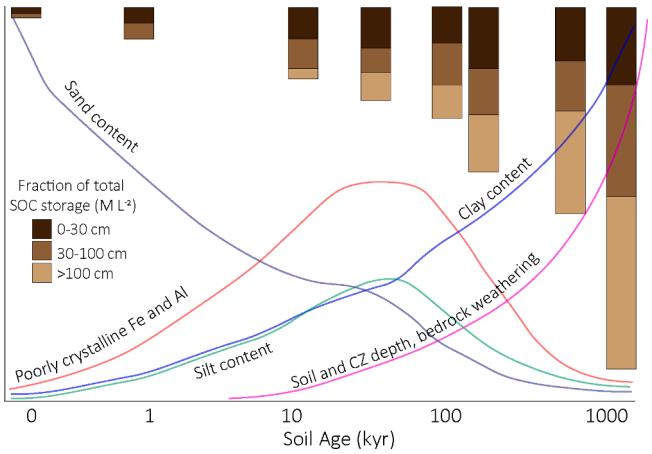

Fig. 9. Schematic of the evolution of soil properties prominence and fractions of SOC stock stored in depth intervals. Soil profile depth (shown by length of column) increases with soil age. As soils age, "deep" SOC below 100 cm, represented by light brown, makes up a greater fraction of the total SOC storage. Poorly crystalline minerals play an important role in SOC storage for soils of ~10 kyr. Increasing soil depth and clay content in the oldest soils creates more space for SOC storage.

Marshall et al., 2015). Cooler and wetter environments tend to form thicker soils and lower OM cycling and decomposition rates. In other settings, the contrast in temperature and water content depending on hillslope aspect, result in higher SOC stocks on north-facing slopes in the northern hemisphere attributed to decreased radiation and contrasting vegetation species and coverage (Chen et al., 2016; Godsey et al., 2018; Lozano-García et al., 2016; Patton et al., 2019).

The controls on soil thickness and mineralogical evolution in the CZ are key, first-order controls on SOC density and stocks. As soils thicken the rate of soil production and weathering decreases (Heimsath et al., 1997). Prior to 100 kyr, the average rate of soil profile deepening is ~0.02 mm/yr. After 120 kyr, the CZ deepens at a minimum average rate of ~0.009 mm/yr. Although SOC density values are low in deep soil horizons (>100 cm), the integration over several meters can often exceed the SOC observed in the upper 30–100 cm in the SRC. Thus, identifying and quantifying the factors that dictate the evolution of soil properties with time and depth and their relationship to SOC dynamics in variable critical zones can inform SOC modeling.

4.3. Beyond Terraces: Broader utility for predicting SOC in eroding landscapes

Incorporating geomorphic context and soil depth estimates into total SOC stock calculations can substantially improve upon previous state-of-the-art predictions and databases. For example, SoilGrids (Poggio et al., 2021), a global soil model that uses data from soil pits and regressions to derive soil properties, only provides data for soil organic carbon stocks in the top 30 cm. For our study area, SoilGrids predicts ~7.5 to 8.0 kgC m^{-2}, which aligns with our measurements in the top 30 cm. However, since soil depth and deep weathering are not accounted for, it neglects deep SOC stocks, which contribute a significant amount of SOC in the older soils.

Furthermore, many recent studies have pointed to the importance of breaking total SOC down into different fractions (Lavallee et al., 2020; Cotrufo et al., 2013, Lehmann and Kleber, 2015). POC, which consists of plant-derived organic matter tends to be relatively short-lived as defined by young ^{14}C ages (<10 year) and is either unprotected or protected via occlusion in soil aggregates (Rasmussen et al., 2005; von Lützow et al., 2007). In contrast, mineral-associated organic carbon (MAOC) is made up of smaller, simpler carbon compounds that can form organo-mineral associations that help to chemically protect carbon from decomposition and disturbance (Eusterhues et al., 2003; Kleber et al., 2015). Tracking and mapping the pedogenic evolution of minerals significant for chemical protection, such as pedogenic Fe and Al oxides, across complex landscapes could improve not only total SOC stocks but fractions MAOC and POC.

Our results show that weathering pathways and the evolution of mineral soil composition impart a strong influence on SOC but the quantitative application of these findings to erosional settings, which dominate much of the Pacific Northwest, is non-trivial. In eroding landscapes, minerals are removed from the soil column through soil transport processes and replenished by soil production from bedrock (Yoo and Mudd, 2008). As a result, determining the erosion rate (or soil residence time) that corresponds with our observed SOC and PCM peak at 34 kyr requires additional analyses. Mudd and Yoo (2010) explore the mineral turnover, age, and residence time using four scenarios with combinations of non-eroding, eroding, mixed, and unmixed soil settings. Because mineral residence time varies with soil production rate and susceptibility to weathering it does not directly equate to soil age (Yoo and Mudd, 2008). Rather, due to downward propagation of the weathering front there is a range of mineral ages that exists in the soil column, with young fresh minerals being introduced at the evolving soil–bedrock interface. Thus, weathering rates that are derived from non-eroding surfaces, such as terraces, will tend to overestimate mineral residence time when directly applied to eroding sites. In the case of our SRC data, if we assume a soil thickness of 1 m and we stipulate that erosion rate is equal to soil thickness divided by the soil residence time (Almond et al., 2007), the average erosion rate necessary to develop a soil with a soil residence time of 30 kyr (which is the soil age associated with peak PCM and SOC content in the shallow soils) would be ~0.03 mm yr^{-1}. However, due to the supply of fresh material from soil production and the removal of older minerals on hillslopes through erosion, a soil with this erosion rate on a hillslope would contain a mineral assemblage with an age distribution skewed younger than a non-eroding soil. Thus, the peak in SOC content and non-crystalline minerals would likely correspond with eroding slopes with erosion rates slower than 0.03 mm yr^{-1}. Systematic analysis and extrapolation of our findings for eroding scenarios is critical for managing landscapes for carbon storage potential but is beyond the scope of this contribution.

5. Conclusions

In this study, we investigated how weathering alters soil geochemistry/mineral assemblages and influences SOC storage. We synthesized previous data (Almond et al., 2007; Lindeburg et al., 2013) from the SRC with new calculations of chemical mass balance. We correlated total SOC stocks and SOC concentrations from three depth intervals with geochemical and physical properties to identify the different soil properties that influence SOC storage at different timescales. We conclude the following:

- As soils age and weather, PCM content in shallow soils peaks at 30 kyr, then declines as amorphous phases ripen to more crystalline Fe and Al pedogenic minerals. SOC density positively correlates with poorly crystalline mineral content.
- Although non-crystalline Al and Fe have a strong correlation with SOC density, their decline with age does not diminish total SOC stocks because deep bedrock weathering and increasing clay content increase to provide space for SOC storage at depth despite low carbon densities. For the oldest soils in our chronosequence (T7), deep SOC (>1 m) constitutes >40% of the SOC inventory despites having <1% carbon for each unit of soil mass.
- The timescale at which SOC densities peak in shallow and deep soils is likely also dependent on climate and parent material which control the rate of weathering.

The ability to predict deep SOC is partly limited by our ability to predict and accurately identify where deep soils exist. Analyzing how

extractable Al and Fe content in addition to soil texture relate to SOC storage with soil age at variable depth, is critical to improving our ability to predict how well (and how much) carbon storage potential exists. Connecting geomorphic theory and soil development models will help inform where deep slowly eroding soils are located and how much SOC could be there. Determining the timescales of weathering products that regulate SOC storage potential motivates new work to couple geomorphic, geochemical, and biological models for land management practices that optimize for SOC storage.

Declaration of Competing Interest

The authors declare that they have no known competing financial interests or personal relationships that could have appeared to influence the work reported in this paper.

Data availability

Data will be made available on request.

Acknowledgment

The authors thank two anonymous reviewers for feedback that improved the manuscript. This work was supported by NSF Division of Earth Sciences (EAR) Climate grant #2136934 awarded to J. Roering and L. Silva.

Appendix

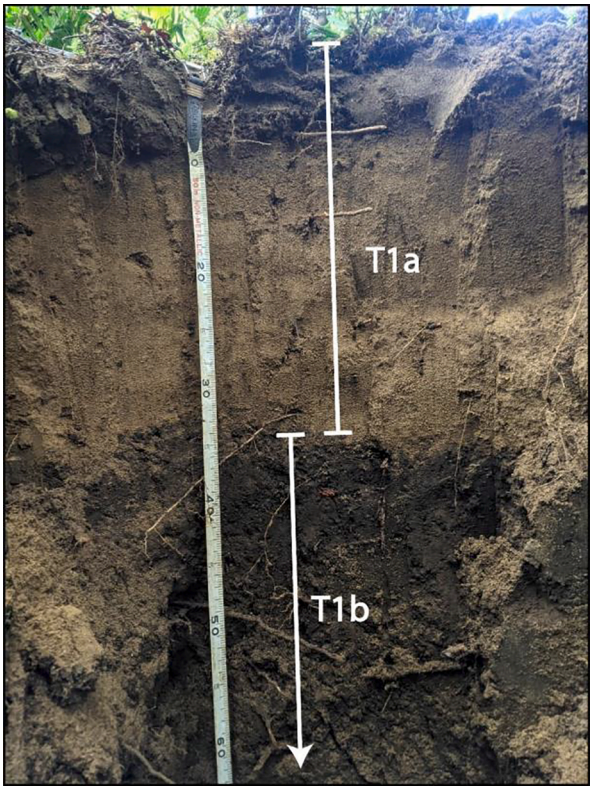

Fig. A1. Annotated photo of Terrace 1. T1a (top) is light in color, coarse, sandy, and relatively unweathered material. T1b is the first buried soil and is much darker in color and composed of finer grained matrix.

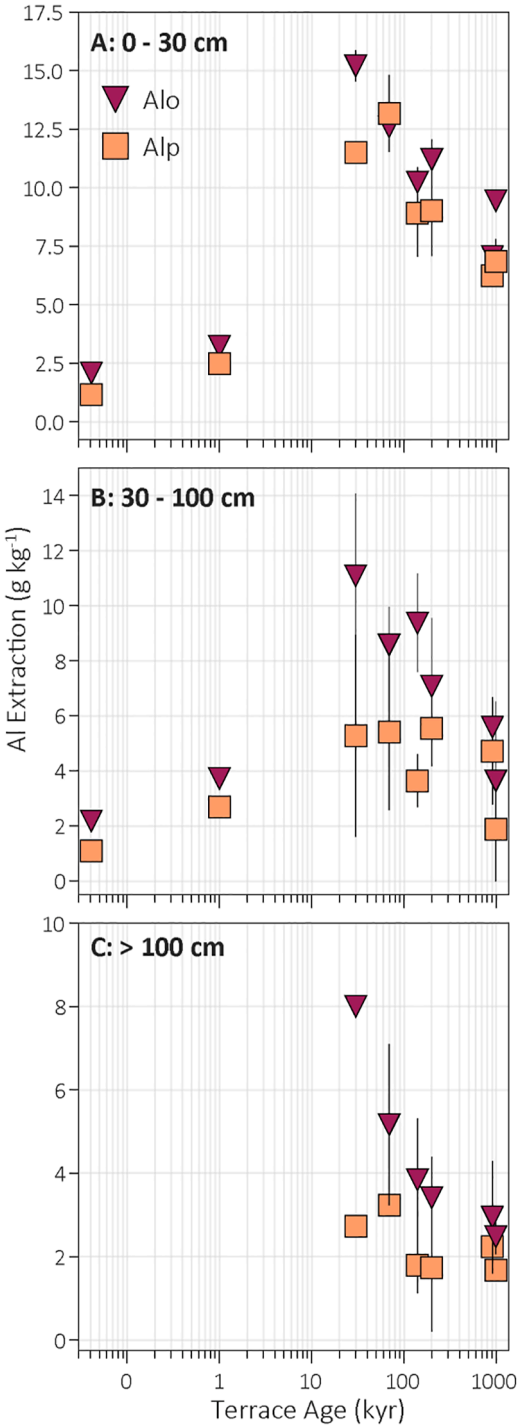

Fig. B1. Depth weighted averages over time for oxalate (Alo - pink triangle), and sodium pyrophosphate (Alp - orange square) extractions for depth intervals 0–30 (A), 30–100 (B), and >100 cm (C). Poorly crystalline Al minerals (PCMs), approximated by Alo, and organo-metal complexes (Alp) peak in both the 0–30 and 30–100 cm intervals ~30–90 kyr, then decline with terrace age.

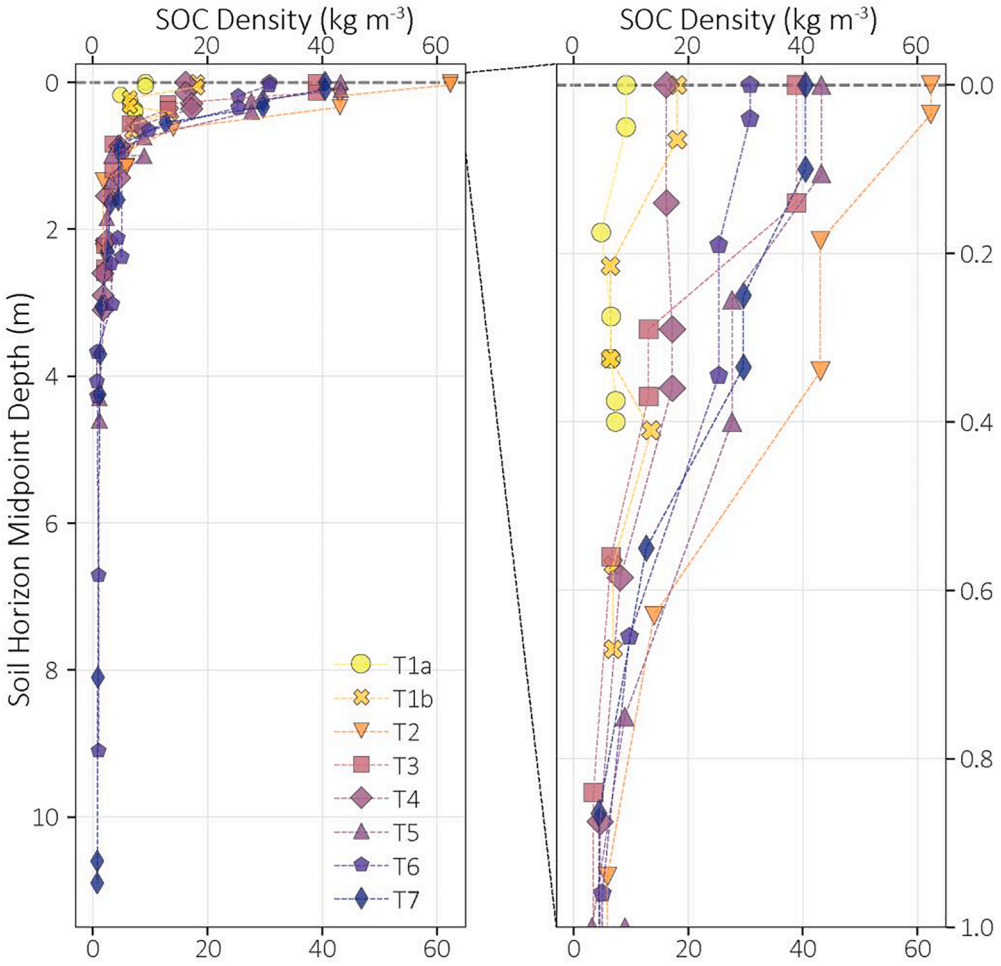

Fig. C1. Calculated SOC density (g cm^{-3}) versus depth (cm) for each terrace. Data are colored and shaped by terrace age. Pull out figure shows soils only in the top 100 cm.

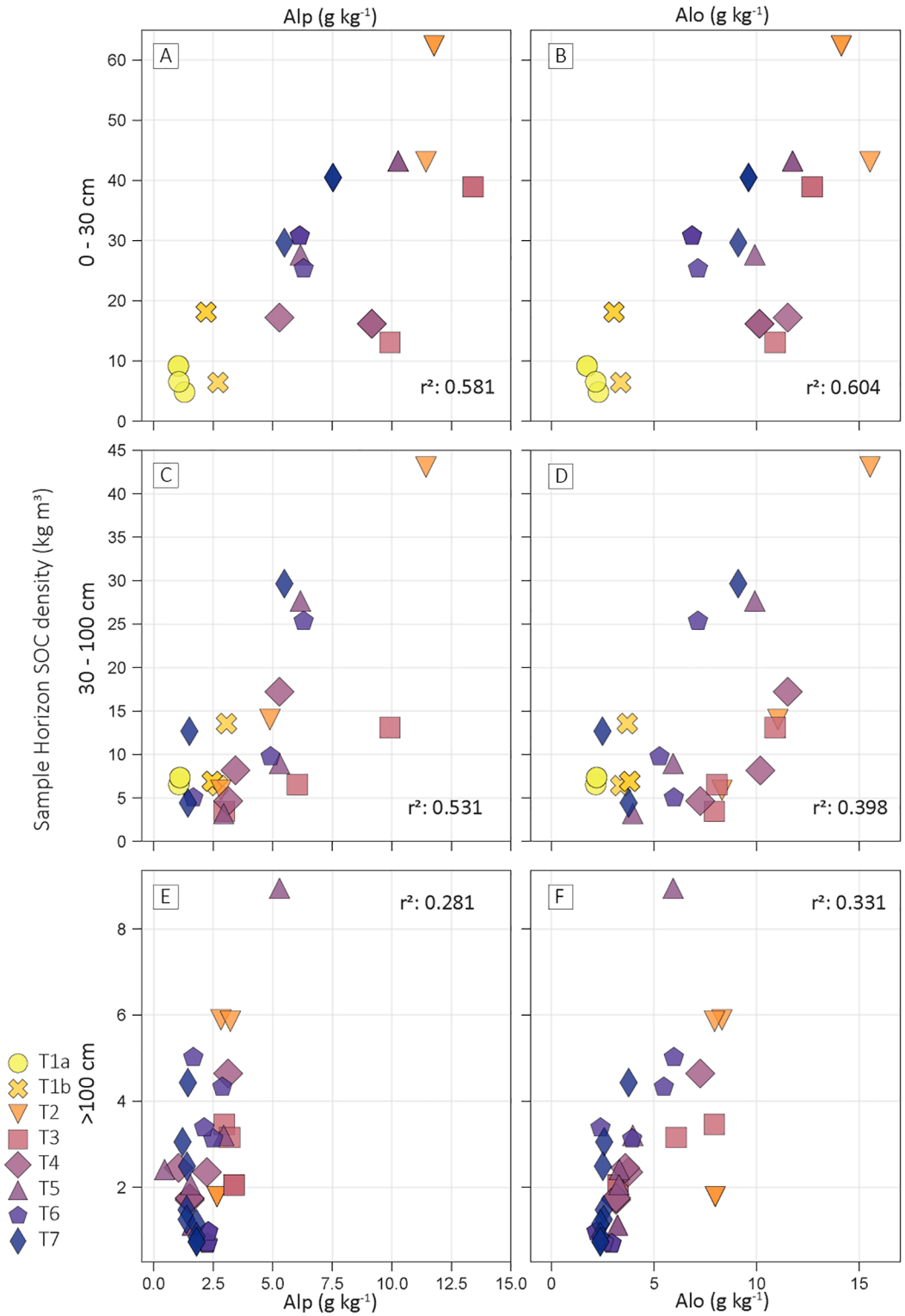

Fig. D1. SOC density (kg m^{-3}) vs Alp (g kg^{-1}) (A, C, and E) and Alo (g kg^{-1}) (B, D, and F) extractions from all terraces and soil layers for soil intervals 0–30 (A and B), 30–100 (C and D), and >100 cm (E and F). Data are colored and shaped by terrace age.

Table A1
Field (bulk density) and lab (pH, CEC, SOC%, SON%, and C:N) measurements from Almond et al. (2007) and Lindeburg et al., 2013 for SOC density (kg m^{-3}), soil depth intervals (0–30, 30–100, and >100 cm) stocks, and total SOC stock (kg m^{-2}) calculations from this study. SOC stocks in Table 2 were calculated by multiplying the horizon interval SOC density by the horizon thickness. Bolded rows were inserted to set firm boundaries for intervals (0–30, 30–100, and >100 cm). Horizons that spanned interval boundaries were split into two and layer thickness was adjusted appropriately.

. Terrace	Age (kyr)	Horizon Increment (cm)	Center Depth (cm)	Layer Thickness Used (cm)	BD (g cm3)	pH	CEC (cmolc kg^{-1})	SOC %	SON %	SOC Density (kg m3)
T1a	0.041	**0–10**	**0**	**0**	**0.91**	**5.4**	**11.49**	**1.00**	**0.04**	**9.16**
		0–10	5	10	0.91	5.4	11.49	1.00	0.04	9.16
		10–25	17.5	15	1.23	5.6	13.16	0.39	0.02	4.81
		25–30	**27.5**	**5**	**1.15**	**5.7**	**15.52**	**0.57**	**0.02**	**6.54**
		30–35	**32.5**	**5**	**1.15**	**5.7**	**15.52**	**0.57**	**0.02**	**6.54**
		35–40	37.5	5	1.16	5.6	15.32	0.63	0.02	7.35
		35–40	**40**	**0**	**1.16**	**5.6**	**15.32**	**0.63**	**0.02**	**7.35**
T1b	1	**0–13**	**0**	**0**	**1.06**	**5.2**	**21.51**	**1.71**	**0.10**	**18.11**
		0–13	6.5	13	1.06	5.2	21.51	1.71	0.10	18.11
		13–30	**21.5**	**17**	**0.49**	**4.9**	**19.82**	**1.32**	**0.09**	**6.42**
		30–35	**32.5**	**5**	**0.49**	**4.9**	**19.82**	**1.32**	**0.09**	**6.42**
		35–47	41	12	1.20	5.1	18.13	1.13	0.08	13.56
		47–67	57	20	1.22	5.5	13.14	0.57	0.02	6.91
		47–67	**67**	**0**	**1.22**	**5.5**	**13.14**	**0.57**	**0.02**	**6.91**
T2	30	**0–7**	**0**	**0**	**0.63**	**4.9**	**47.92**	**9.91**	**0.45**	**62.34**
		0–7	3.5	7	0.63	4.9	47.92	9.91	0.45	62.34
		7–30	**18.5**	**23**	**0.89**	**4.8**	**39.41**	**4.84**	**0.20**	**43.07**
		30–38	**34**	**8**	**0.89**	**4.8**	**39.41**	**4.84**	**0.20**	**43.07**
		38–88	63	50	1.04	4.9	24.54	1.36	0.04	14.02
		88–100	**94**	**12**	**1.10**	**4.9**	**24.41**	**0.53**	**0.00**	**5.89**
		100–109	**104.5**	**9**	**1.10**	**4.9**	**24.41**	**0.53**	**0.00**	**5.89**
		109–122	115.5	13	1.30	4.9	22.57	0.45	*	5.86
		122–146	134	24	1.19	5.3	17.48	0.15	*	1.78
		146–230	188	84	1.19	5.3	17.48	0.15	*	1.78
		146–230	**230**	**0**	**1.19**	**5.3**	**17.48**	**0.15**	*	**1.78**
T3	69	**0–28**	**0**	**0**	**1.01**	**5**	**29.53**	**3.87**	**0.10**	**38.91**
		0–28	14	28	1.01	5	29.53	3.87	0.10	38.91
		28–30	**29**	**2**	**1.23**	**5**	**17.54**	**1.06**	**0.02**	**13.08**
		30–44	**37**	**14**	**1.23**	**5**	**17.54**	**1.06**	**0.02**	**13.08**
		44–68	56	24	1.15	5	16.22	0.57	*	6.53
		68–100	**84**	**32**	**1.16**	**5.1**	**15.56**	**0.30**	*	**3.46**
		100–113	**106.5**	**13**	**1.16**	**5.1**	**15.56**	**0.30**	*	**3.46**
		113–200	156.5	87	1.34	4.8	18.38	0.24	*	3.16
		200–245	222.5	45	1.47	4.9	12.59	0.14	*	2.05
		245–260	252.5	15	1.47	4.9	12.59	0.14	*	2.05
		245–260	**260**	**0**	**1.47**	**4.9**	**12.59**	**0.14**	*	**2.05**
T4	140	**0–28**	**0**	**0**	**0.99**	**5**	**29.32**	**1.64**	**0.04**	**16.19**
		0–28	14	28	0.99	5	29.32	1.64	0.04	16.19
		28–30	**29**	**2**	**1.00**	**4.9**	**20.61**	**1.71**	**0.03**	**17.21**
		30–42	**36**	**12**	**1.00**	**4.9**	**20.61**	**1.71**	**0.03**	**17.21**
		42–75	58.5	33	1.13	5.2	16.58	0.72	*	8.17
		75–100	**87.5**	**25**	**1.43**	**5.2**	**14.86**	**0.33**	*	**4.64**
		100–120	**110**	**20**	**1.43**	**5.2**	**14.86**	**0.33**	*	**4.64**
		120–190	155	70	1.14	5.1	15.43	0.21	*	2.35
		190–240	215	50	1.34	5.1	18.81	0.18	*	2.45
		240–270	255	30	1.43	5.1	24.50	0.12	*	1.71
		270–310	290	40	1.46	5	22.98	0.12	*	1.75
		270–310	**310**	**0**	**1.46**	**5**	**22.98**	**0.12**	*	**1.75**
T5	200	**0–21**	**0**	**0**	**0.82**	**5.2**	**29.74**	**5.27**	**0.15**	**43.23**
		0–21	10.5	21	0.82	5.2	29.74	5.27	0.15	43.23
		21–30	**25.5**	**9**	**1.04**	**5.1**	**22.95**	**2.65**	**0.05**	**27.64**
		30–50	**40**	**20**	**1.04**	**5.1**	**22.95**	**2.65**	**0.05**	**27.64**
		50–100	75	50	1.20	5.2	17.68	0.74	0.01	8.94
		100–100	**100**	**0**	**1.26**	**5**	**16.37**	**0.25**	*	**3.21**
		100–100	**100**	**0**	**1.20**	**5.2**	**17.68**	**0.74**	**0.01**	**8.94**
		100–170	135	70	1.26	5	16.37	0.25	*	3.21
		170–200	185	30	1.30	4.7	14.82	0.19	*	2.41
		200–400	300	200	1.34	4.7	16.35	0.15	*	2.06
		400–460	430	60	1.33	4.9	10.56	0.08	*	1.12
		400–460	**460**	**0**	**1.33**	**4.9**	**10.56**	**0.08**	*	**1.12**
T6	908	**0–8**	**0**	**0**	**1.12**	**5**	**20.66**	**2.74**	**0.06**	**30.79**
		0–8	4	8	1.12	5	20.66	2.74	0.06	30.79
		8–30	**19**	**22**	**1.10**	**5.2**	**21.33**	**2.31**	**0.04**	**25.34**
		30–39	34.5	9	1.10	5.2	21.33	2.31	0.04	25.34
		39–92	65.5	53	1.01	5.3	20.94	0.97	0.02	9.74
		92–100	**96**	**8**	**1.04**	**4.8**	**17.54**	**0.48**	*	**5.01**
		100–192	**146**	**92**	**1.04**	**4.8**	**17.54**	**0.48**	*	**5.01**
		192–232	212	40	1.35	5.1	20.91	0.32	*	4.33
		232–262	247	30	1.16	4.9	20.37	0.27	*	3.12
		262–342	302	80	1.55	4.6	19.84	0.22	*	3.38

(*continued on next page*)

Table A1 (*continued*)

. Terrace	Age (kyr)	Horizon Increment (cm)	Center Depth (cm)	Layer Thickness Used (cm)	BD (g cm3)	pH	CEC (cmolc kg^{-1})	SOC %	SON %	SOC Density (kg m3)
		342–392	367	50	1.42	4.8	21.37	0.05	*	0.68
		392–422	407	30	1.20	4.8	20.06	0.06	*	0.69
		422–432	427	10	1.14	4.8	22.98	0.06	*	0.72
		432–910	671	478	1.23	4.7	21.43	0.08	*	0.97
		432–910	**910**	**0**	**1.23**	**4.7**	**21.43**	**0.08**	*	**0.97**
T7	990	**0–20**	**0**	**0**	**0.78**	**4.9**	**33.91**	**5.22**	**0.18**	**40.48**
		0–20	10	20	0.78	4.9	33.91	5.22	0.18	40.48
		20–30	**25**	**10**	**1.02**	**5**	**27.70**	**2.90**	**0.09**	**29.65**
		30–37	**33.5**	**7**	**1.02**	**5**	**27.70**	**2.90**	**0.09**	**29.65**
		37–73	55	36	1.11	5.2	14.69	1.14	0.03	12.68
		73–100	**86.5**	**27**	**1.23**	**4.9**	**14.38**	**0.36**	**0.02**	**4.43**
		100–140	**120**	**40**	**1.23**	**4.9**	**14.38**	**0.36**	**0.02**	**4.43**
		140–190	165	50	1.17	5	15.25	0.26	0.00	3.05
		190–270	230	80	1.29	5	16.15	0.19	0.01	2.49
		270–340	305	70	1.40	4.9	16.43	0.11	*	1.48
		340–400	370	60	1.34	4.8	17.29	0.09	*	1.25
		400–500	450	100	1.31	4.8	18.13	0.09	*	1.15
		500–950	725	450	1.30	4.7	19.40	0.07	0	0.85
		950–1090	1020	140	1.72	4.9	20.92	0.04	0.02	0.73
		950–1090	**1090**	**0**	**1.72**	**4.9**	**20.92**	**0.04**	**0.02**	**0.73**

Table B1
Fe extraction data for T1a-T7. Bolded rows were inserted to set firm boundaries for intervals (0–30, 30–100, and >100 cm). Horizons that spanned interval boundaries were split into two and layer thickness was adjusted appropriately.

Terrace	Age (kyr)	Horizon Increment (cm)	Center Depth (cm)	Layer Thickness Used (cm)	Fep (g kg^{-1})	DWA	STD	Feo (g kg^{-1})	DWA	STD	Fed (g kg^{-1})	DWA	STD
T1a	0.041	**0–10**	**0**	**0**	**0.519**	0.402	0.102	**2.033**	2.406	0.504	**4.894**	4.85	0.26
		0–10	5	10	0.519			2.033			4.894		
		10–25	17.5	15	0.284			2.368			4.648		
		25–30	**27.5**	**5**	**0.523**			**3.265**			**5.367**		
		30–35	**32.5**	**5**	**0.523**	0.539	0.015	**3.265**	3.298	0.031	**5.367**	5.38	0.01
		35–40	37.5	5	0.555			3.331			5.394		
		35–40	**40**	**0**	**0.555**			**3.331**			**5.394**		
T1b	1	**0–13**	**0**	**0**	**1.883**	2.102	0.18	**4.491**	4.454	0.03	**8.959**	9.33	0.31
		0–13	6.5	13	1.883			4.491			8.959		
		13–30	**21.5**	**17**	**2.269**			**4.426**			**9.614**		
		30–35	**32.5**	**5**	**2.269**	1.608	0.67	**4.426**	3.432	0.87	**9.614**	8.555	1.17
		35–47	41	12	2.377			4.34			9.945		
		47–67	57	20	0.982			2.639			7.457		
		47–67	**67**	**0**	**0.982**			**2.639**			**7.457**		
T2	30	**0–7**	**0**	**0**	**6.058**	4.368	1.04	**11.204**	12.18	0.6	**22.563**	22.75	0.11
		0–7	3.5	7	6.058			11.204			22.563		
		7–30	**18.5**	**23**	**3.854**			**12.475**			**22.802**		
		30–38	**34**	**8**	**3.854**	1.392	1.39	**12.475**	8.942	2.75	**22.802**	22.72	0.72
		38–88	63	50	1.163			9.145			23.022		
		88–100	**94**	**12**	**0.706**			**5.741**			**21.393**		
		100–109	**104.5**	**9**	**0.706**	0.24	0.2	**5.741**	3.722	0.89	**21.393**	6.66	6.28
		109–122	115.5	13	0.255			3.341			8.753		
		122–146	134	24	0.199			3.6			5.18		
		146–230	188	84	0.199			3.6			5.18		
		146–230	**230**	**0**	**0.199**			**3.6**			**5.18**		
Terrace	Age (kyr)	Horizon Increment (cm)	Center Depth (cm)	Layer Thickness Used (cm)	Fep (g kg^{-1})	DWA	STD	Feo (g kg^{-1})	DWA	STD	Fed (g kg^{-1})	DWA	STD
T3	69	**0–28**	**0**	**0**	**1.848**	1.76	0.62	**9.805**	9.505	2.12	**26.533**	26.71	1.27
		0–28	14	28	1.848			9.805			26.533		
		28–30	**29**	**2**	**0.532**			**5.307**			**29.217**		
		30–44	**37**	**14**	**0.532**	0.399	0.08	**5.307**	3.852	0.86	**29.217**	30.88	0.99
		44–68	56	24	0.387			3.648			30.95		
		68–100	**84**	**32**	**0.35**			**3.369**			**31.55**		
		100–113	**106.5**	**13**	**0.35**	0.581	0.18	**3.369**	2.365	0.54	**31.55**	25.64	2.54
		113–200	156.5	87	0.478			2.484			25.011		
		200–245	222.5	45	0.78			1.976			25.284		
		245–260	252.5	15	0.78			1.976			25.284		
		245–260	**260**	**0**	**0.78**			**1.976**			**25.284**		

(*continued on next page*)

Table B1 (*continued*)

Terrace	Age (kyr)	Horizon Increment (cm)	Center Depth (cm)	Layer Thickness Used (cm)	Fep (g kg^{-1})	DWA	STD	Feo (g kg^{-1})	DWA	STD	Fed (g kg^{-1})	DWA	STD
T4	140	**0–28**	**0**	**0**	**2.772**	2.644	0.91	**8.912**	8.785	0.9	**33.406**	33.43	0.15
		0–28	14	28	2.772			8.912			33.406		
		28–30	**29**	**2**	**0.847**			**7.013**			**33.73**		
		30–42	**36**	**12**	**0.847**	0.403	0.28	**7.013**	5.513	0.89	**33.73**	38.09	3.35
		42–75	58.5	33	0.171			5.395			36.812		
		75–100	**87.5**	**25**	**0.497**			**4.95**			**41.86**		
		100–120	**110**	**20**	**0.497**	0.767	0.26	**4.95**	4.735	0.55	**41.86**	41.31	0.66
		120–190	155	70	1.168			3.857			42.2		
		190–240	215	50	0.743			5.76			40.855		
		240–270	255	30	0.461			4.819			40.594		
		270–310	290	40	0.461			4.819			40.594		
		270–310	**310**	**0**	**0.461**			**4.819**			**40.594**		
Terrace	Age (kyr)	Horizon Increment (cm)	Center Depth (cm)	Layer Thickness Used (cm)	Fep (g kg^{-1})	DWA	STD	Feo (g kg^{-1})	DWA	STD	Fed (g kg^{-1})	DWA	STD
T5	200	**0–21**	**0**	**0**	**5.179**	4.254	1.45	**7.331**	6.71	0.98	**45.97**	45.69	0.44
		0–21	10.5	21	5.179			7.331			45.97		
		21–30	**25.5**	**9**	**2.097**			**5.26**			**45.028**		
		30–50	**40**	**20**	**2.097**	1.108	0.74	**5.26**	5.21	0.31	**45.028**	55.88	6.52
		50–100	75	50	0.712			5.19			60.22		
		100–100	**100**	**0**	**0.389**			**4.563**			**56.897**		
		100–100	**100**	**0**	**0.712**	0.383	0.27	**5.19**	4.09	0.59	**60.22**	43.17	10.9
		100–170	**135**	**70**	**0.389**			**4.563**			**56.897**		
		170–200	185	30	0.368			4.416			47.787		
		200–400	300	200	0			4.047			40.883		
		400–460	430	60	0			3.519			32.445		
		400–460	**460**	**0**	**0**			**3.519**			**32.445**		
T6	908	**0–8**	**0**	**0**	**2.355**	2.389	0.02	**3.135**	3.097	0.02	**47.787**	52.73	3.18
		0–8	4	8	2.355			3.135			47.787		
		8–30	**19**	**22**	**2.401**			**3.083**			**54.529**		
		30–39	**34.5**	**9**	**2.401**	1.05	0.85	**3.083**	3.268	0.21	**54.529**	69.64	7.75
		39–92	65.5	53	0.917			3.252			73.369		
		92–100	**96**	**8**	**0.408**			**3.582**			**61.912**		
		100–192	**146**	**92**	**0.408**	0.223	0.09	**3.582**	2.45	0.85	**61.912**	31.65	11
		192–232	212	40	0.18			1.93			36.08		
		232–262	247	30	0.266			1.473			37.884		
		262–342	302	80	0.353			1.017			39.688		
		342–392	367	50	0.173			1.136			31.458		
		392–422	407	30	0.173			1.136			31.458		
		422–432	427	10	0.175			1.971			27.647		
		432–910	671	478	0.176			2.806			23.836		
		432–910	**910**	**0**	**0.176**			**2.806**			**23.836**		
	Age (kyr)	Horizon Increment (cm)	Center Depth (cm)	Layer Thickness Used (cm)	Fep (g kg^{-1})	DWA	STD	Feo (g kg^{-1})	DWA	STD	Fed (g kg^{-1})	DWA	STD
T7	990	**0–20**	**0**	**0**	**2.726**	2.455	0.38	**4.197**	3.965	0.33	**43.528**	47.72	5.93
		0–20	10	20	2.726			4.197			43.528		
		20–30	**25**	**10**	**1.913**			**3.5**			**56.102**		
		30–37	**33.5**	**7**	**1.913**	0.599	0.73	**3.5**	2.362	0.76	**56.102**	44.43	13.5
		37–73	55	36	0.67			1.68			29.972		
		73–100	**86.5**	**27**	**0.164**			**2.976**			**60.681**		
		100–140	**120**	**40**	**0.164**	0.164	0.05	**2.976**	2.48	0.3	**60.681**	54.21	3.04
		140–190	165	50	0			3.05			56.299		
		190–270	230	80	0			2.233			50.037		
		270–340	305	70	0			2.179			51.163		
		340–400	370	60	0			2.179			51.163		
		400–500	450	100	0			2.495			54.747		
		500–950	725	450	0			2.495			54.747		
		950–1090	1020	140	0			2.495			54.747		
		950–1090	**1090**	**0**	**0**			**2.495**			**54.747**		

Table C1
Al extraction data for T1a-T7. Bolded rows were inserted to set firm boundaries for intervals (0–30, 30–100, and >100 cm). Horizons that spanned interval boundaries were split into two and layer thickness was adjusted appropriately.

Terrace	Age (kyr)	Horizon Increment (cm)	Center Depth (cm)	Layer Thickness Used (cm)	Alp (g kg^{-1})	DWA	STD	Alo (g kg^{-1})	DWA	STD
T1a	0.041	**0–10**	**0**	**0**	1.038	1.172	0.110	1.734	2.084	0.251
		0–10	5	10	1.038			1.734		
		10–25	17.5	15	1.298			2.292		
		25–30	**27.5**	**5**	1.059			2.161		
		30–35	**32.5**	**5**	1.059	1.081	0.021	2.161	2.183	0.020
		35–40	37.5	5	1.103			2.204		
		35–40	**40**	**0**	1.103			2.204		
T1b	1	**0–13**	**0**	**0**	2.202	2.483	0.234	3.05	3.233	0.152
		0–13	6.5	13	2.202			3.05		
		13–30	**21.5**	**17**	2.698			3.373		
		30–35	**32.5**	**5**	2.698	2.683	0.246	3.373	3.715	0.180
		35–47	41	12	3.057			3.695		
		47–67	57	20	2.455			3.813		
		47–67	**67**	**0**	2.455			3.813		
T2	30	**0–7**	**0**	**0**	11.769	11.509	0.160	14.13	15.203	0.659
		0–7	3.5	7	11.769			14.13		
		7–30	**18.5**	**23**	11.43			15.529		
		30–38	**34**	**8**	11.43	5.276	3.670	15.529	11.083	2.975
		38–88	63	50	4.88			11.037		
		88–100	**94**	**12**	2.824			8.313		
		100–109	**104.5**	**9**	2.824	2.723	0.218	8.313	8.005	0.135
		109–122	115.5	13	3.218			7.953		
		122–146	134	24	2.655			7.985		
		146–230	188	84	2.655			7.985		
		146–230	**230**	**0**	2.655			7.985		
Terrace	Age (kyr)	Horizon Increment (cm)	Center Depth (cm)	Layer Thickness Used (cm)	Alp (g kg^{-1})	DWA	STD	Alo (g kg^{-1})	DWA	STD
T3	69	**0–28**	**0**	**0**	13.407	13.174	1.645	12.721	12.600	0.853
		0–28	14	28	13.407			12.721		
		28–30	**29**	**2**	9.918			10.911		
		30–44	**37**	**14**	9.918	5.409	2.843	10.911	8.578	1.372
		44–68	56	24	6.028			8.064		
		68–100	**84**	**32**	2.971			7.942		
		100–113	**106.5**	**13**	2.971	3.240	0.160	7.942	5.169	1.936
		113–200	156.5	87	3.188			6.081		
		200–245	222.5	45	3.375			3.247		
		245–260	252.5	15	3.375			3.247		
		245–260	**260**	**0**	3.375			3.247		
T4	140	**0–28**	**0**	**0**	9.159	8.901	1.827	10.139	10.231	0.652
		0–28	14	28	9.159			10.139		
		28–30	**29**	**2**	5.283			11.523		
		30–42	**36**	**12**	5.283	3.640	0.953	11.523	9.363	1.786
		42–75	58.5	33	3.434			10.181		
		75–100	**87.5**	**25**	3.123			7.247		
		100–120	**110**	**20**	3.123	1.795	0.679	7.247	3.846	1.467
		120–190	155	70	2.238			3.742		
		190–240	215	50	1.042			3.6		
		240–270	255	30	1.511			3.155		
		270–310	290	40	1.511			3.155		
		270–310	**310**	**0**	1.511			3.155		

Terrace	Age (kyr)	Horizon Increment (cm)	Center Depth (cm)	Layer Thickness Used (cm)	Alp (g kg^{-1})	DWA	STD	Alo (g kg^{-1})	DWA	STD
T5	200	**0–21**	**0**	**0**	10.259	9.030	1.932	11.759	11.205	0.870
		0–21	10.5	21	10.259			11.759		
		21–30	**25.5**	**9**	6.161			9.914		
		30–50	**40**	**20**	6.161	5.533	1.359	9.914	7.070	2.475
		50–100	75	50	5.282			5.933		
		100–100	**100**	**0**	2.941			3.963		
		100–100	**100**	**0**	5.282	1.739	1.537	5.933	3.416	0.977
		100–170	**135**	**70**	2.941			3.963		
		170–200	185	30	0.458			3.312		
		200–400	300	200	1.546			3.297		
		400–460	430	60	1.62			3.226		
		400–460	**460**	**0**	1.62			3.226		
T6	908	**0–8**	**0**	**0**	6.132	6.251	0.076	6.857	7.065	0.134
		0–8	4	8	6.132			6.857		
		8–30	**19**	**22**	6.294			7.141		
		30–39	**34.5**	**9**	6.294	4.715	1.940	7.141	5.589	0.773
		39–92	65.5	53	4.908			5.268		
		92–100	**96**	**8**	1.664			5.97		
		100–192	**146**	**92**	1.664	2.237	0.301	5.97	2.948	1.344
		192–232	212	40	2.88			5.478		
		232–262	247	30	2.499			3.935		
		262–342	302	80	2.118			2.392		
		342–392	367	50	2.25			2.93		
		392–422	407	30	2.25			2.93		
		422–432	427	10	2.272			2.563		
		432–910	671	478	2.294			2.196		
		432–910	**910**	**0**	2.294			2.196		
Terrace	Age (kyr)	Horizon Increment (cm)	Center Depth (cm)	Layer Thickness Used (cm)	Alp (g kg^{-1})	DWA	STD	Alo (g kg^{-1})	DWA	STD
T7	990	**0–20**	**0**	**0**	7.526	6.846	0.962	9.608	9.440	0.238
		0–20	10	20	7.526			9.608		
		20–30	**25**	**10**	5.486			9.104		
		30–37	**33.5**	**7**	5.486	1.873	1.895	9.104	3.642	2.866
		37–73	55	36	1.498			2.488		
		73–100	**86.5**	**27**	1.437			3.764		
		100–140	**120**	**40**	1.437	1.669	0.225	3.764	2.482	0.415
		140–190	165	50	1.212			2.572		
		190–270	230	80	1.398			2.508		
		270–340	305	70	1.385			2.552		
		340–400	370	60	1.385			2.552		
		400–500	450	100	1.8			2.385		
		500–950	725	450	1.8			2.385		
		950–1090	1020	140	1.8			2.385		
		950–1090	**1090**	**0**	1.8			2.385		

Table D1
Correlation coefficients for analyzed variables for the all soil samples (T1-T7 and all soil depths).

	SOC (kg m3)	SOC %	OC (g kg^{-1})	CEC (cmolc kg^{-1})	Fep (g kg^{-1})	Alp (g kg^{-1})	Feo (g kg^{-1})	Alo (g kg^{-1})	Fed (g kg^{-1})	Ald (g kg^{-1})	0.5xFeo + Alo (g kg^{-1})	Sand %	Silt %	Clay %	pH	Age (kyr)
SOC (kg m3)																
SOC %	0.972															
OC (g kg^{-1})	0.972	1														
CEC (cmolc kg^{-1})	0.814	0.85	0.85													
Fep (g kg^{-1})	0.912	0.921	0.921	0.791												
Alp (g kg^{-1})	0.853	0.802	0.802	0.757	0.779											
Feo (g kg^{-1})	0.703	0.695	0.695	0.737	0.701	0.781										
Alo (g kg^{-1})	0.768	0.729	0.729	0.716	0.681	0.881	0.813									
Fed (g kg^{-1})	0.016	−0.008	−0.008	0.08	−0.035	0.059	−0.058	0.007								
Ald (g kg^{-1})	0.719	0.676	0.676	0.676	0.66	0.847	0.735	0.867	0.438							
0.5xFeo + Alo (g kg^{-1})	0.779	0.747	0.747	0.748	0.712	0.887	0.893	0.988	−0.01	0.865						
Sand %	−0.185	−0.17	−0.17	−0.253	−0.13	−0.306	−0.108	−0.368	−0.735	−0.606	−0.311					
Silt %	0.216	0.28	0.28	0.511	0.265	0.341	0.309	0.379	0.199	0.414	0.372	−0.58				
Clay %	0.099	0.043	0.043	0.009	0.003	0.174	−0.049	0.227	0.78	0.496	0.161	−0.879	0.122			
pH	0.016	−0.027	−0.027	−0.264	0.028	−0.101	−0.054	−0.067	−0.45	−0.253	−0.066	0.531	−0.691	−0.243		
Age (kyr)	−0.097	−0.106	−0.106	0.022	−0.206	−0.173	−0.451	−0.275	0.651	−0.044	−0.331	−0.521	0.195	0.521	−0.435	
Center Depth (cm)	−0.493	−0.425	−0.425	−0.183	−0.469	−0.411	−0.391	−0.48	0.253	−0.367	−0.475	0.009	0.327	−0.202	−0.457	0.46

Table D2
Correlation coefficients for analyzed variables for soils in the 0–30 cm soil interval for T1-T7.

	SOC (kg m3)	SOC %	OC (g kg^{-1})	CEC (cmolc kg^{-1})	Fep (g kg^{-1})	Alp (g kg^{-1})	Feo (g kg^{-1})	Alo (g kg^{-1})	Fed (g kg^{-1})	Ald (g kg^{-1})	0.5xFeo + Alo (g kg^{-1})	Sand %	Silt %	Clay %	pH	Age (kyr)
SOC (kg m3)																
SOC %	0.958															
OC (g kg^{-1})	0.958	1														
CEC (cmolc kg^{-1})	0.891	0.911	0.911													
Fep (g kg^{-1})	0.844	0.878	0.878	0.854												
Alp (g kg^{-1})	0.762	0.673	0.673	0.768	0.635											
Feo (g kg^{-1})	0.636	0.632	0.632	0.797	0.645	0.832										
Alo (g kg^{-1})	0.777	0.701	0.701	0.808	0.649	0.937	0.839									
Fed (g kg^{-1})	0.44	0.271	0.271	0.301	0.343	0.451	0.054	0.514								
Ald (g kg^{-1})	0.767	0.66	0.66	0.748	0.67	0.913	0.711	0.957	0.714							
0.5xFeo + Alo (g kg^{-1})	0.764	0.705	0.705	0.832	0.669	0.939	0.911	0.989	0.404	0.921						
Sand %	−0.444	−0.321	−0.321	−0.289	−0.371	−0.589	−0.185	−0.645	−0.862	−0.852	−0.531					
Silt %	0.681	0.652	0.652	0.705	0.722	0.747	0.64	0.889	0.433	0.925	0.847	−0.758				
Clay %	0.155	0.001	0.001	−0.081	0.023	0.316	−0.184	0.297	0.921	0.565	0.164	−0.891	0.379			
pH	−0.559	−0.506	−0.506	−0.658	−0.466	−0.641	−0.561	−0.714	−0.471	−0.698	−0.695	0.562	−0.634	−0.356		
Age (kyr)	0.228	0.1	0.1	0.078	0.044	0.026	−0.378	0.061	0.768	0.245	−0.058	−0.518	−0.033	0.758	−0.288	
Center Depth (cm)	−0.378	−0.382	−0.382	−0.283	−0.395	−0.166	−0.123	−0.002	0.051	−0.031	−0.036	−0.021	−0.08	0.086	0.077	−0.061

Table D3
Correlation coefficients for analyzed variables for soils in the 30–100 cm soil interval for T1-T7.

	SOC (kg m3)	SOC %	OC (g kg^{-1})	CEC (cmolc kg^{-1})	Fep (g kg^{-1})	Alp (g kg^{-1})	Feo (g kg^{-1})	Alo (g kg^{-1})	Fed (g kg^{-1})	Ald (g kg^{-1})	0.5xFeo + Alo (g kg^{-1})	Sand %	Silt %	Clay %	pH	Age (kyr)
SOC (kg m3)																
SOC %	0.982															
OC (g kg^{-1})	0.982	1														
CEC (cmolc kg^{-1})	0.836	0.879	0.879													
Fep (g kg^{-1})	0.823	0.866	0.866	0.757												
Alp (g kg^{-1})	0.729	0.718	0.718	0.695	0.549											
Feo (g kg^{-1})	0.56	0.612	0.612	0.778	0.492	0.655										
Alo (g kg^{-1})	0.631	0.626	0.626	0.716	0.365	0.817	0.788									
Fed (g kg^{-1})	0.105	0.065	0.065	0.126	−0.117	0.217	−0.058	0.212								
Ald (g kg^{-1})	0.548	0.52	0.52	0.602	0.25	0.785	0.575	0.87	0.637							
0.5xFeo + Alo (g kg^{-1})	0.639	0.648	0.648	0.761	0.412	0.81	0.874	0.988	0.153	0.832						
Sand %	−0.279	−0.273	−0.273	−0.354	−0.112	−0.407	−0.201	−0.486	−0.862	−0.789	−0.432					
Silt %	0.583	0.594	0.594	0.699	0.494	0.716	0.784	0.863	0.285	0.817	0.877	−0.6				
Clay %	0.08	0.068	0.068	0.118	−0.082	0.175	−0.103	0.205	0.908	0.588	0.134	−0.937	0.282			
pH	−0.287	−0.339	−0.339	−0.519	−0.264	−0.454	−0.512	−0.607	−0.427	−0.661	−0.608	0.787	−0.798	−0.594		
Age (kyr)	0.162	0.121	0.121	0.045	−0.023	−0.06	−0.367	−0.109	0.725	0.206	−0.178	−0.652	−0.069	0.811	−0.221	
Center Depth (cm)	−0.571	−0.571	−0.571	−0.297	−0.546	−0.345	−0.131	−0.123	0.427	0.086	−0.13	−0.356	0.044	0.408	−0.247	0.153

Table D4
Correlation coefficients for analyzed variables for soils >100 cm soil interval for T1-T7.

	SOC (kg m3)	SOC %	OC (g kg^{-1})	CEC (cmolc kg^{-1})	Fep (g kg^{-1})	Alp (g kg^{-1})	Feo (g kg^{-1})	Alo (g kg^{-1})	Fed (g kg^{-1})	Ald (g kg^{-1})	0.5xFeo + Alo (g kg^{-1})	Sand %	Silt %	Clay %	pH	Age (kyr)
SOC (kg m3)																
SOC %	0.989															
OC (g kg^{-1})	0.989	1														
CEC (cmolc kg^{-1})	0.008	0.021	0.021													
Fep (g kg^{-1})	0.395	0.381	0.381	−0.07												
Alp (g kg^{-1})	0.53	0.503	0.503	−0.04	0.45											
Feo (g kg^{-1})	0.397	0.411	0.411	0.068	0.36	−0.023										
Alo (g kg^{-1})	0.575	0.593	0.593	0.024	0.246	0.506	0.399									
Fed (g kg^{-1})	0.136	0.141	0.141	−0.088	−0.146	−0.354	0.056	−0.503								
Ald (g kg^{-1})	0.76	0.759	0.759	−0.169	0.555	0.292	0.605	0.394	0.398							
0.5xFeo + Alo (g kg^{-1})	0.603	0.621	0.621	0.039	0.309	0.429	0.613	0.969	−0.418	0.502						
Sand %	−0.51	−0.536	−0.536	−0.129	−0.125	−0.2	0.18	−0.237	−0.397	−0.365	−0.158					
Silt %	−0.44	−0.459	−0.459	0.593	−0.153	0.07	−0.427	−0.332	−0.532	−0.669	−0.414	0.009				
Clay %	0.663	0.694	0.694	−0.203	0.187	0.133	0.072	0.375	0.616	0.66	0.351	−0.851	−0.533			
pH	0.273	0.269	0.269	−0.1	0.261	0.326	0.459	0.61	−0.252	0.359	0.649	−0.109	−0.394	0.299		
Age (kyr)	−0.257	−0.23	−0.23	0.233	−0.595	−0.375	−0.613	−0.571	0.509	−0.402	−0.657	−0.395	0.306	0.174	−0.496	
Center Depth (cm)	−0.598	−0.59	−0.59	0.251	−0.462	−0.259	−0.323	−0.556	0.148	−0.603	−0.566	0.412	0.443	−0.581	−0.422	0.51

References

Almond, P., Roering, J., Hales, T.C., 2007. Using soil residence time to delineate spatial and temporal patterns of transient landscape response. J. Geophys. Res. 112, F03S17. https://doi.org/10.1029/2006JF000568.

Anderson, R.S., Anderson, S.P., Tucker, G.E., 2013. Rock damage and regolith transport by frost: an example of climate modulation of the geomorphology of the critical zone: Rock Damage and Regolith Transport by Frost. Earth Surface Processes Landforms 38, 299–316. https://doi.org/10.1002/esp.3330.

Anderson, S.P., Dietrich, W.E., 2002. Weathering profiles, mass-balance analysis, and rates of solute loss: Linkages between weathering and erosion in a small, steep catchment. Geolog. Soc. Am. Bull. 16 https://doi.org/10.1130/0016-7606(2002)114<1143:WPMBAA>2.0.CO;2.

Baisden, W.T., Amundson, R., Brenner, D.L., Cook, A.C., Kendall, C., Harden, J.W., 2002. A multiisotope C and N modeling analysis of soil organic matter turnover and transport as a function of soil depth in a California annual grassland soil chronosequence: Organic Matter Dynamics in a Soil Chronosequence. Global Biogeochem. Cycles 16 (4), 82-1–82-26.

Baldock, J.A., Skjemstad, J.O., 2000. Role of the soil matrix and minerals in protecting natural organic materials against biological attack. Organic Geochem. 31, 697–710. https://doi.org/10.1016/S0146-6380(00)00049-8.

Batjes, N.H., 2014. Total carbon and nitrogen in the soils of the world. Eur. J. Soil Sci. 65, 10–21. https://doi.org/10.1111/ejss.12114_2.

Beschta, R.L., 1978. Long-term patterns of sediment production following road construction and logging in the Oregon Coast Range. Water Resour. Res. 14, 1011–1016. https://doi.org/10.1029/WR014i006p01011.

Birkeland, P.W., 1992. Quaternary soil chronosequences in various environments — extremely arid to humid tropical, in: Developments in Earth Surface Processes. Elsevier, pp. 261–281. https://doi.org/10.1016/B978-0-444-89198-3.50016-7.

Blanco-Canqui, H., Lal, R., 2004. Mechanisms of Carbon Sequestration in Soil Aggregates. Critical Rev. Plant Sci. 23, 481–504. https://doi.org/10.1080/07352680490886842.

Brimhall, G.H., Dietrich, W.E., 1987. Constitutive mass balance relations between chemical composition, volume, density, porosity, and strain in metasomatic hydrochemkai systems: Results on weathering and pedogenesis 21. https://doi.org/10.1016/0016-7037(87)90070-6.

Brimhall, G.H., Christopher., J.L., Ford, C., Bratt, J., Taylor, G., Warin, O., 1991. Quantitative geochemical approach to pedogenesis: importance of parent material reduction, volumetric expansion, and eolian influx in lateritization. Geoderma 51 (1-4), 51–91.

Chadwick, O.A., Chorover, J., 2001. The chemistry of pedogenic thresholds. Geoderma 100, 321–353. https://doi.org/10.1016/S0016-7061(01)00027-1.

Chadwick, O.A., Brimhall, G.H., Hendricks, D.M., 1990. From a black to a gray box - a mass balance interpretation of pedogenesis.pdf. Geomorphology 3, 369–390. https://doi.org/10.1016/0169-555X(90)90012-F.

Chan, M.A., Dott, R.H., 1983. Shelf and Deep-Sea Sedimentation in Eocene Forearc Basin, Western Oregon–Fan or Non-Fan? Bulletin 67.

Chen, L.-F., He, Z.-B., Du, J., Yang, J.-J., Zhu, X., 2016. Patterns and environmental controls of soil organic carbon and total nitrogen in alpine ecosystems of northwestern China. CATENA 137, 37–43. https://doi.org/10.1016/j.catena.2015.08.017.

Chorover, J., Amistadi, M.K., Chadwick, O.A., 2004. Surface charge evolution of mineral-organic complexes during pedogenesis in Hawaiian basalt. Geochimica et Cosmochimica Acta 68, 4859–4876. https://doi.org/10.1016/j.gca.2004.06.005.

Conant, R.T., Ryan, M.G., Ågren, G.I., Birge, H.E., Davidson, E.A., Eliasson, P.E., Evans, S.E., Frey, S.D., Giardina, C.P., Hopkins, F.M., Hyvönen, R., Kirschbaum, M.U.F., Lavallee, J.M., Leifeld, J., Parton, W.J., Megan Steinweg, J., Wallenstein, M.D., Martin Wetterstedt, J.Å., Bradford, M.A., 2011. Temperature and soil organic matter decomposition rates - synthesis of current knowledge and a way forward. Glob. Change Biol. 17, 3392–3404. https://doi.org/10.1111/j.1365-2486.2011.02496.x.

Cotrufo, M.F., Wallenstein, M.D., Boot, C.M., Denef, K., Paul, E., 2013. The Microbial Efficiency-Matrix Stabilization (MEMS) framework integrates plant litter decomposition with soil organic matter stabilization: do labile plant inputs form stable soil organic matter? Glob Change Biol 19, 988–995. https://doi.org/10.1111/gcb.12113.

Dietrich, W.E., Dunne, T., 1978. Sediment budget for a small catchment in mountainous terrain. Z. Geomorphol. N.F. 29, 191–206.

Doetterl, S., Berhe, A.A., Nadeu, E., Wang, Z., Sommer, M., Fiener, P., 2016. Erosion, deposition and soil carbon: A review of process-level controls, experimental tools and models to address C cycling in dynamic landscapes. Earth-Sci. Rev. 154, 102–122. https://doi.org/10.1016/j.earscirev.2015.12.005.

Doetterl, S., Berhe, A.A., Arnold, C., Bodé, S., Fiener, P., Finke, P., Fuchslueger, L., Griepentrog, M., Harden, J.W., Nadeu, E., Schnecker, J., Six, J., Trumbore, S., Van Oost, K., Vogel, C., Boeckx, P., 2018. Links among warming, carbon and microbial dynamics mediated by soil mineral weathering. Nature Geoscience 11, 589–593. https://doi.org/10.1038/s41561-018-0168-7.

Eusterhues, K., Rumpel, C., Kleber, M., Kögel-Knabner, I., 2003. Stabilisation of soil organic matter by interactions with minerals as revealed by mineral dissolution and oxidative degradation. Organic Geochemistry 34, 1591–1600. https://doi.org/10.1016/j.orggeochem.2003.08.007.

Fontaine, S., Barot, S., Barré, P., Bdioui, N., Mary, B., Rumpel, C., 2007. Stability of organic carbon in deep soil layers controlled by fresh carbon supply. Nature 450, 277–280. https://doi.org/10.1038/nature06275.

Garcia Arredondo, M., Lawrence, C.R., Schulz, M.S., Tfaily, M.M., Kukkadapu, R., Jones, M.E., Boye, K., Keiluweit, M., 2019. Root-driven weathering impacts on mineral-organic associations in deep soils over pedogenic time scales. Geochimica et Cosmochimica Acta 263, 68–84. https://doi.org/10.1016/j.gca.2019.07.030.

Gavin, D.G., Brubaker, L.B., Lertzman, K.P., 2003. Holocene Fire History of a Coastal Temperate Rain Forest Based on Soil Charcoal Radiocarbon Dates. Ecology 84, 186–201. https://doi.org/10.1890/0012-9658(2003)084[0186:HFHOAC]2.0.CO;2.

Godsey, S.E., Marks, D., Kormos, P.R., Seyfried, M.S., Enslin, C.L., Winstral, A.H., McNamara, J.P., Link, T.E., 2018. Eleven years of mountain weather, snow, soil moisture and streamflow data from the rain–snow transition zone – the Johnston Draw catchment, Reynolds Creek Experimental Watershed and Critical Zone Observatory, USA 10, 1207–1216, https://doi.org/10.5194/essd-10-1207-2018, 2018.

Georgiou, K., Jackson, R.B., Vindušková, O., Abramoff, R.Z., Ahlström, A., Feng, W., Harden, J.W., Pellegrini, A.F.A., Polley, H.W., Soong, J.L., Riley, W.J., Torn, M.S., 2022. Global stocks and capacity of mineral-associated soil organic carbon. Nat Commun 13, 3797. https://doi.org/10.1038/s41467-022-31540-9.

Graham, R., Rossi, A., Hubbert, R., 2010. Rock to regolith conversion: Producing hospitable substrates for terrestrial ecosystems. GSAT 4–9. https://doi.org/10.1130/GSAT57A.1.

Guggenberger, G., Kaiser, K., 2003. Dissolved organic matter in soil: challenging the paradigm of sorptive preservation. Geoderma 113, 293–310. https://doi.org/10.1016/S0016-7061(02)00366-X.

Harden, J.W., 1982. A quantitative index of soil development from field descriptions: Examples from a chronosequence in central California. Geoderma 28, 1–28. https://doi.org/10.1016/0016-7061(82)90037-4.

Harper, R.J., Tibbett, M., 2013. The hidden organic carbon in deep mineral soils. Plant Soil 368, 641–648. https://doi.org/10.1007/s11104-013-1600-9.

Harr, R.D., 1981. Some characteristics and consequences of snowmelt during rainfall in western Oregon. Journal of Hydrology 53, 277–304. https://doi.org/10.1016/0022-1694(81)90006-8.

Heimsath, A.M., Dietrich, W.E., Nishiizumi, K., Finkel, R.C., 1997. The soil production function and landscape equilibrium. Nature 388, 358–361. https://doi.org/10.1038/41056.

Heimsath, A.M., Dietrich, W.E., Nishiizumi, K., Finkel, R.C., 2001. Stochastic processes of soil production and transport: erosion rates, topographic variation and cosmogenic nuclides in the Oregon Coast Range. Earth Surf. Process. Landforms 26, 531–552. https://doi.org/10.1002/esp.209.

Heller, P., Dickinson, W., 1985. Submarine Ramp Facies Model for Delta-Fed. Sand-Rich Turbidite Systems. Bulletin 69. https://doi.org/10.1306/AD462B37-16F7-11D7-8645000102C1865D.

Hemingway, J.D., Rothman, D.H., Grant, K.E., Rosengard, S.Z., Eglinton, T.I., Derry, L.A., Galy, V.V., 2019. Mineral protection regulates long-term global preservation of natural organic carbon. Nature 570, 228–231. https://doi.org/10.1038/s41586-019-1280-6.

Jobbágy, E.G., Jackson, R.B., 2000. The vertical distribution of soil organic carbon and its relation to climate and vegetation. Ecological Appl. 10, 423–436. https://doi.org/10.1890/1051-0761(2000)010[0423:TVDOSO]2.0.CO;2.

Kaiser, K., Guggenberger, G., 2003. Mineral surfaces and soil organic matter: Mineral surfaces and soil organic matter. Eur. J. Soil Sci. 54, 219–236. https://doi.org/10.1046/j.1365-2389.2003.00544.x.

Kaiser, K., Kalbitz, K., 2012. Cycling downwards – dissolved organic matter in soils. Soil Biol. Biochem. 52, 29–32. https://doi.org/10.1016/j.soilbio.2012.04.002.

Kelsey, H.M., Ticknor, R.L., Bockheim, J.G., Mitchell, E., 1996. Quaternary upper plate deformation in coastal Oregon. Geol. Soc. Am. Bull. 108, 843–860. https://doi.org/10.1130/0016-7606(1996)108<0843:QUPDIC>2.3.CO;2.

Kirschbaum, M.U.F., 2000. Will changes in soil organic carbon act as a positive or negative feedback on global warming? Biogeochemistry 48, 21–51. https://doi.org/10.1023/A:1006238902976.

Kleber, M., Bourg, I.C., Coward, E.K., Hansel, C.M., Myneni, S.C.B., Nunan, N., 2021. Dynamic interactions at the mineral–organic matter interface. Nat. Rev. Earth Environ. 2, 402–421. https://doi.org/10.1038/s43017-021-00162-y.

Kleber, M., Eusterhues, K., Keiluweit, M., Mikutta, C., Mikutta, R., Nico, P.S., 2015. Mineral–Organic Associations: Formation, Properties, and Relevance in Soil Environments, in: Advances in Agronomy. Elsevier, pp. 1–140. https://doi.org/10.1016/bs.agron.2014.10.005.

Kögel-Knabner, I., Guggenberger, G., Kleber, M., Kandeler, E., Kalbitz, K., Scheu, S., Eusterhues, K., Leinweber, P., 2008. Organo-mineral associations in temperate soils: Integrating biology, mineralogy, and organic matter chemistry. Z. Pflanzenernähr. Bodenk. 171, 61–82. https://doi.org/10.1002/jpln.200700048.

Kramer, M.G., Chadwick, O.A., 2016. Controls on carbon storage and weathering in volcanic soils across a high-elevation climate gradient on Mauna Kea, Hawaii. Ecology 97, 2384–2395. https://doi.org/10.1002/ecy.1467.

Lal, R., 2018. Digging deeper: A holistic perspective of factors affecting soil organic carbon sequestration in agroecosystems. Glob. Change Biol. 24, 3285–3301. https://doi.org/10.1111/gcb.14054.

Lavallee, J.M., Soong, J.L., Cotrufo, M.F., 2020. Conceptualizing soil organic matter into particulate and mineral-associated forms to address global change in the 21st century. Glob. Change Biol. 26, 261–273. https://doi.org/10.1111/gcb.14859.

Lawrence, C.R., Harden, J.W., Xu, X., Schulz, M.S., Trumbore, S.E., 2015. Long-term controls on soil organic carbon with depth and time: A case study from the Cowlitz River Chronosequence, WA USA. Geoderma 247–248, 73–87. https://doi.org/10.1016/j.geoderma.2015.02.005.

Lawrence, C.R., Schulz, M.S., Masiello, C.A., Chadwick, O.A., Harden, J.W., 2021. The trajectory of soil development and its relationship to soil carbon dynamics. Geoderma 403, 115378. https://doi.org/10.1016/j.geoderma.2021.115378.

Le Quéré, C., Moriarty, R., Andrew, R.M., Peters, G.P., Ciais, P., Friedlingstein, P., Jones, S.D., Sitch, S., Tans, P., Arneth, A., Boden, T.A., Bopp, L., Bozec, Y.,

Canadell, J.G., Chini, L.P., Chevallier, F., Cosca, C.E., Harris, I., Hoppema, M., Houghton, R.A., House, J.I., Jain, A.K., Johannessen, T., Kato, E., Keeling, R.F., Kitidis, V., Klein Goldewijk, K., Koven, C., Landa, C.S., Landschützer, P., Lenton, A., Lima, I.D., Marland, G., Mathis, J.T., Metzl, N., Nojiri, Y., Olsen, A., Ono, T., Peng, S., Peters, W., Pfeil, B., Poulter, B., Raupach, M.R., Regnier, P., Rödenbeck, C., Saito, S., Salisbury, J.E., Schuster, U., Schwinger, J., Séférian, R., Segschneider, J., Steinhoff, T., Stocker, B.D., Sutton, A.J., Takahashi, T., Tilbrook, B., van der Werf, G. R., Viovy, N., Wang, Y.-P., Wanninkhof, R., Wiltshire, A., Zeng, N., 2015. Global carbon budget 2014. Earth Syst. Sci. Data 7, 47–85. https://doi.org/10.5194/essd-7-47-2015.

Lebedeva, M.I., Brantley, S.L., 2013. Exploring geochemical controls on weathering and erosion of convex hillslopes: beyond the empirical regolith production function: Hillslope evolution and regolith thickness. Earth Surf. Process. Landforms 38, 1793–1807. https://doi.org/10.1002/esp.3424.

Lehmann, J., Hansel, C.M., Kaiser, C., Kleber, M., Maher, K., Manzoni, S., Nunan, N., Reichstein, M., Schimel, J.P., Torn, M.S., Wieder, W.R., Kögel-Knabner, I., 2020. Persistence of soil organic carbon caused by functional complexity. Nat. Geosci. 13, 529–534. https://doi.org/10.1038/s41561-020-0612-3.

Lehmann, J., Kleber, M., 2015. The contentious nature of soil organic matter. Nature 528, 60–68. https://doi.org/10.1038/nature16069.

Lilienfein, J., Qualls, R.G., Uselman, S.M., Bridgham, S.D., 2003. Soil formation and organic matter accretion in a young andesitic chronosequence at Mt. Shasta. California. Geoderma 116, 249–264. https://doi.org/10.1016/S0016-7061(03)00086-7.

Lindeburg, K.S., Almond, P., Roering, J.J., Chadwick, O.A., 2013. Pathways of soil genesis in the Coast Range of Oregon, USA. Plant Soil 367, 57–75. https://doi.org/10.1007/s11104-012-1566-z.

Long, C.J., Whitlock, C., Bartlein, P.J., Millspaugh, S.H., 1998. A 9000-year fire history from the Oregon Coast Range, based on a high-resolution charcoal study. Can. J. For. Res. 28 (5), 774–787.

Lovell, J.P.B., 1969. Tyee Formation: Undeformed Turbidites and their Lateral Equivalents: Mineralogy and Paleogeography. Geol. Soc. Am. Bull. 80, 9. https://doi.org/10.1130/0016-7606(1969)80[9:TFUTAT]2.0.CO;2.

Lozano-García, B., Parras-Alcántara, L., Brevik, E.C., 2016. Impact of topographic aspect and vegetation (native and reforested areas) on soil organic carbon and nitrogen budgets in Mediterranean natural areas. Sci. Total Environ. 544, 963–970. https://doi.org/10.1016/j.scitotenv.2015.12.022.

Mainka, M., Summerauer, L., Wasner, D., Garland, G., Griepentrog, M., Berhe, A.A., Doetterl, S., 2022. Soil geochemistry as a driver of soil organic matter composition: insights from a soil chronosequence. Biogeosciences 19, 1675–1689. https://doi.org/10.5194/bg-19-1675-2022.

Marshall, J.A., Roering, J.J., Bartlein, P.J., Gavin, D.G., Granger, D.E., Rempel, A.W., Praskievicz, S.J., Hales, T.C., 2015. Frost for the trees: Did climate increase erosion in unglaciated landscapes during the late Pleistocene? Sci. Adv. 1, e1500715.

Marshall, J.A., Roering, J.J., Gavin, D.G., Granger, D.E., 2017. Late Quaternary climatic controls on erosion rates and geomorphic processes in western Oregon, USA. Geolog. Soc. Am. Bull. 129, 715–731. https://doi.org/10.1130/B31509.1.

Masiello, C.A., Chadwick, O.A., Southon, J., Torn, M.S., Harden, J.W., 2004. Weathering controls on mechanisms of carbon storage in grassland soils: Weathering controls on carbon storage. Global Biogeochem. Cycles 18 (4), n/a–n/a.

McKeague, J.A., 1967. An evaluation of 0.1 *M* Pyrophosphate and pyrophosphate-dithionite in comparison with oxalate as extractants of the accumulation products in podzols and some other soils. Can. J. Soil. Sci. 47, 95–99. https://doi.org/10.4141/cjss67-017.

McKeague, J.A., Day, J.H., 1966. Dithionite- and oxalate-extractable Fe and Al as aids in differentiating various classes of soils. Can. J. Soil. Sci. 46, 13–22. https://doi.org/10.4141/cjss66-003.

Mehra, O.P., Jackson, M.L., 1958. Iron Oxide Removal from Soils and Clays by a Dithionite-Citrate System Buffered with Sodium Bicarbonate. Clays and Clay Minerals 7, 317–327. https://doi.org/10.1346/CCMN.1958.0070122.

Mikutta, R., Kleber, M., Jahn, R., 2005. Poorly crystalline minerals protect organic carbon in clay subfractions from acid subsoil horizons. Geoderma 128, 106–115. https://doi.org/10.1016/j.geoderma.2004.12.018.

Minasny, B., Malone, B.P., McBratney, A.B., Angers, D.A., Arrouays, D., Chambers, A., Chaplot, V., Chen, Z.-S., Cheng, K., Das, B.S., Field, D.J., Gimona, A., Hedley, C.B., Hong, S.Y., Mandal, B., Marchant, B.P., Martin, M., McConkey, B.G., Mulder, V.L., O'Rourke, S., Richer-de-Forges, A.C., Odeh, I., Padarian, J., Paustian, K., Pan, G., Poggio, L., Savin, I., Stolbovoy, V., Stockmann, U., Sulaeman, Y., Tsui, C.-C., Vågen, T.-G., van Wesemael, B., Winowiecki, L., 2017. Soil carbon 4 per mille. Geoderma 292, 59–86. https://doi.org/10.1016/j.geoderma.2017.01.002.

Mitchell, C.E., Vincent, P., Weldon, R.J., Richards, M.A., 1994. Present-day vertical deformation of the Cascadia Margin, Pacific Northwest, United States. J. Geophys. Res. 99 (B6), 12257–12277.

Montgomery, D.R., 2001. Slope Distributions, Threshold Hillslopes, and Steady-state Topography. Am J Sci 301, 432–454. https://doi.org/10.2475/ajs.301.4-5.432.

Moreland, K., Tian, Z., Berhe, A.A., McFarlane, K.J., Hartsough, P., Hart, S.C., Bales, R., O'Geen, A.T., 2021. Deep in the Sierra Nevada critical zone: saprock represents a large terrestrial organic carbon stock. Environ. Res. Lett. 16 (12), 124059 https://doi.org/10.1088/1748-9326/ac3bfe.

Mudd, S.M., Yoo, K., 2010. Reservoir theory for studying the geochemical evolution of soils. Journal of Geophysical Research 115. https://doi.org/10.1029/2009JF001591.

Parfitt, R., Childs, C., 1988. Estimation of forms of Fe and Al - a review, and analysis of contrasting soils by dissolution and Mossbauer methods. Soil Res. 26, 121. https://doi.org/10.1071/SR9880121.

Patching WR (1987) Soil Survey of Lane County Area, Oregon. United States Department of Agriculture, Soil Conservation Service, Washington, D.C.

Patton, N.R., Lohse, K.A., Seyfried, M.S., Godsey, S.E., Parsons, S.B., 2019. Topographic controls of soil organic carbon on soil-mantled landscapes. Scientific Reports 9. https://doi.org/10.1038/s41598-019-42556-5.

Penserini, B.D., Roering, J.J., Streig, A., 2017. A morphologic proxy for debris flow erosion with application to the earthquake deformation cycle, Cascadia Subduction Zone, USA. Geomorphology 282, 150–161. https://doi.org/10.1016/j.geomorph.2017.01.018.

Poggio, L., de Sousa, L.M., Batjes, N.H., Heuvelink, G.B.M., Kempen, B., Ribeiro, E., Rossiter, D., 2021. SoilGrids 2.0: producing soil information for the globe with quantified spatial uncertainty. SOIL 7, 217–240. https://doi.org/10.5194/soil-7-217-2021.

Rasmussen, C., Torn, M.S., Southard, R.J., 2005. Mineral Assemblage and Aggregates Control Carbon Dynamics in a California Conifer Forest. Soil Sci. Soc. Am. J. 69, 1711–1721. https://doi.org/10.2136/sssaj2005.0040.

Rasmussen, C., Heckman, K., Wieder, W.R., Keiluweit, M., Lawrence, C.R., Berhe, A.A., Blankinship, J.C., Crow, S.E., Druhan, J.L., Hicks Pries, C.E., Marin-Spiotta, E., Plante, A.F., Schädel, C., Schimel, J.P., Sierra, C.A., Thompson, A., Wagai, R., 2018. Beyond clay: towards an improved set of variables for predicting soil organic matter content. Biogeochemistry 137, 297–306. https://doi.org/10.1007/s10533-018-0424-3.

Rempe, D.M., Dietrich, W.E., 2014. A bottom-up control on fresh-bedrock topography under landscapes. Proc. National Acad. Sci. 111, 6576–6581. https://doi.org/10.1073/pnas.1404763111.

Reneau, S.L., Dietrich, W.E., 1991. Erosion rates in the southern oregon coast range: Evidence for an equilibrium between hillslope erosion and sediment yield. Earth Surf. Process. Landforms 16, 307–322. https://doi.org/10.1002/esp.3290160405.

Riebe, C.S., Hahm, W.J., Brantley, S.L., 2017. Controls on deep critical zone architecture: a historical review and four testable hypotheses: Four Testable Hypotheses about the Deep Critical Zone. Earth Surf. Process. Landforms 42, 128–156. https://doi.org/10.1002/esp.4052.

Rumpel, C., Kögel-Knabner, I., 2011. Deep soil organic matter—a key but poorly understood component of terrestrial C cycle. Plant Soil 338, 143–158. https://doi.org/10.1007/s11104-010-0391-5.

Sanderman, J., Amundson, R., 2008. A comparative study of dissolved organic carbon transport and stabilization in California forest and grassland soils. Biogeochemistry 89 (3), 309–327.

Sanderman, J., Baldock, J.A., Amundson, R., 2008. Dissolved organic carbon chemistry and dynamics in contrasting forest and grassland soils. Biogeochemistry 89, 181–198. https://doi.org/10.1007/s10533-008-9211-x.

Schmidt, M.W.I., Torn, M.S., Abiven, S., Dittmar, T., Guggenberger, G., Janssens, I.A., Kleber, M., Kögel-Knabner, I., Lehmann, J., Manning, D.A.C., Nannipieri, P., Rasse, D.P., Weiner, S., Trumbore, S.E., 2011. Persistence of soil organic matter as an ecosystem property. Nature 478, 49–56. https://doi.org/10.1038/nature10386.

Schrumpf, M., Kaiser, K., Guggenberger, G., Persson, T., Kögel-Knabner, I., Schulze, E.-D., 2013. Storage and stability of organic carbon in soils as related to depth, occlusion within aggregates, and attachment to minerals. Biogeosciences 10, 1675–1691. https://doi.org/10.5194/bg-10-1675-2013.

Silva, L.C.R., Lambers, H., 2021. Soil-plant-atmosphere interactions: structure, function, and predictive scaling for climate change mitigation. Plant Soil 461, 5–27. https://doi.org/10.1007/s11104-020-04427-1.

Six, J., Paustian, K., Elliott, E.T., Combrink, C., 2000. Soil Structure and Organic Matter I. Distribution of Aggregate-Size Classes and Aggregate-Associated Carbon. Soil Sci. Soc. Am. J. 64, 681–689. https://doi.org/10.2136/sssaj2000.642681x.

Slessarev, E.W., Chadwick, O.A., Sokol, N.W., Nuccio, E.E., Pett-Ridge, J., 2022. Rock weathering controls the potential for soil carbon storage at a continental scale. Biogeochemistry 157, 1–13. https://doi.org/10.1007/s10533-021-00859-8.

Slim, M., Perron, J.T., Martel, S.J., Singha, K., 2015. Topographic stress and rock fracture: a two-dimensional numerical model for arbitrary topography and preliminary comparison with borehole observations: Topographic Stress and Rock Fracture. Earth Surf. Process. Landforms 40, 512–529. https://doi.org/10.1002/esp.3646.

St. Clair, J., Moon, S., Holbrook, W.S., Perron, J.T., Riebe, C.S., Martel, S.J., Carr, B., Harman, C., Singha, K., Richter, D.deB., 2015. Geophysical imaging reveals topographic stress control of bedrock weathering. Science 350 (6260), 534–538.

Sweeney, K.E., Roering, J.J., Almond, P., Reckling, T., 2012. How steady are steady-state landscapes? Using visible–near-infrared soil spectroscopy to quantify erosional variability. Geology 40, 807–810. https://doi.org/10.1130/G33167.1.

Tarnocai, C., Canadell, J.G., Schuur, E.A.G., Kuhry, P., Mazhitova, G., Zimov, S., 2009. Soil organic carbon pools in the northern circumpolar permafrost region. Global Biogeochem. Cycles 23 (2), n/a–n/a.

Torn, M.S., Trumbore, S.E., Chadwick, O.A., Vitousek, P.M., Hendricks, D.M., 1997. Mineral control of soil organic carbon storage and turnover. Nature 389, 170–173. https://doi.org/10.1038/38260.

Totsche, K.U., Amelung, W., Gerzabek, M.H., Guggenberger, G., Klumpp, E., Knief, C., Lehndorff, E., Mikutta, R., Peth, S., Prechtel, A., Ray, N., Kögel-Knabner, I., 2018. Microaggregates in soils. J. Plant Nutr. Soil Sci. 181, 104–136. https://doi.org/10.1002/jpln.201600451.

von Lützow, M., Kögel-Knabner, I., Ekschmitt, K., Flessa, H., Guggenberger, G., Matzner, E., Marschner, B., 2007. SOM fractionation methods: Relevance to functional pools and to stabilization mechanisms. Soil Biol. Biochem. 39, 2183–2207. https://doi.org/10.1016/j.soilbio.2007.03.007.

Vreeken, W.J., 1975. Principal kinds of chronosequences and their significance in soil history. J. Soil Sci. 26, 378–394. https://doi.org/10.1111/j.1365-2389.1975.tb01962.x.

Walker, L.R., Wardle, D.A., Bardgett, R.D., Clarkson, B.D., 2010. The use of chronosequences in studies of ecological succession and soil development: Chronosequences, succession and soil development. J. Ecol. 98, 725–736. https://doi.org/10.1111/j.1365-2745.2010.01664.x.

Wei, Y., Wu, X., Xia, J., Shen, X., Cai, C., Reigosa, M., 2016. Variation of Soil Aggregation along the Weathering Gradient: Comparison of Grain Size Distribution under Different Disruptive Forces. PLoS ONE 11 (8), e0160960.

Wells, R., Bukry, D., Friedman, R., Pyle, D., Duncan, R., Haeussler, P., Wooden, J., 2014. Geologic history of Siletzia, a large igneous province in the Oregon and Washington Coast Range: Correlation to the geomagnetic polarity time scale and implications for a long-lived Yellowstone hotspot. Geosphere 10, 692–719. https://doi.org/10.1130/GES01018.1.

Wells, R.E., Heller, P.L., 1988. The relative contribution of accretion, shear, and extension to Cenozoic tectonic rotation in the Pacific Northwest. Geolog. Soc. Am. Bull. 100, 325–338. https://doi.org/10.1130/0016-7606(1988)100<0325:TRCOAS>2.3.CO;2.

Wells, R.E., McCaffrey, R., 2013. Steady rotation of the Cascade arc. Geology 41, 1027–1030. https://doi.org/10.1130/G34514.1.

Wells, R.E., Weaver, C.S., Blakely, R.J., 1998. Fore-arc migration in Cascadia and its neotectonic significance. Geol 26, 759. https://doi.org/10.1130/0091-7613(1998)026<0759:FAMICA>2.3.CO;2.

Yoo, K., Jelinski, N., 2016. Soil Mantled Hillslopes: Intersections of Geomorphology, Soil Science, and Ecology. In: Johnson, E.A., Martin, Y.E. (Eds.), A Biogeoscience Approach to Ecosystems. Cambridge University Press, pp. 180–214.

Yoo, K., Mudd, S.M., 2008. Discrepancy between mineral residence time and soil age: Implications for the interpretation of chemical weathering rates. Geology 36, 35. https://doi.org/10.1130/G24285A.1.

Yost, J.L., Hartemink, A.E., 2020. How deep is the soil studied – an analysis of four soil science journals. Plant Soil 452, 5–18. https://doi.org/10.1007/s11104-020-04550-z.